Christopher Fradler

Investigations on the Layer Formation in Nanocomposite Solar Cells

DIPLOMARBEIT

zur Erlangung des akademischen Grades eines Diplom Ingenuers der technischen Wissenschaften

erreicht an der

Technischen Universität Graz

Betreuer:
O. Univ.-Prof. DI Dr. Franz Stelzer
Assoc. Prof. DI Dr. Gregor Trimmel

Institut für Chemische Technologie von Materialien
Technische Universität Graz

2010

STATUTORY DECLARATION

I declare that I have authored this thesis independently, that I have not used other than the declared sources / resources, and that I have explicitly marked all material which has been quoted either literally or by content from the used sources.

Graz, August 27th, 2010 Christopher Fradler

Für meine Eltern

ABSTRACT

Investigations on the Layer Formation in Nanocomposite Solar Cells

Within this work alternative assembly strategies for organic and inorganic-organic nanocomposite solar cells have been investigated. The active layer of these solar cells consists either of a mixture of two organic semiconductors or of a mixture of one inorganic with one organic semiconductor. In the first part, two different assembly strategies of organic solar cells have been investigated using as example the donor-acceptor system poly(3-hexylthiophene-2,5-diyl) (P3HT) / [6,6]-phenyl-C_{61}-butyric acid methyl ester (PCBM). The first strategy uses the most common assembly, which starts with the transparent electrode, glass-supported indium tin oxide (ITO), followed by a polymer interface layer of poly(3,4-ethylenedioxythiophene) poly(styrenesulfonate (PEDOT:PSS), the active layer (P3HT/PCBM) and finally the aluminium electrode. The second approach, the “back side assembly”, starts at the aluminium electrode and ends with PEDOT:PSS topped with a thin layer of 5 nm gold, which was used as transparent electrode.

The second part focuses on the preparation of porous copper indium disulfide layers for the application as inorganic acceptor material in nanocomposite solar cells. After a possible infiltration step with an organic polymer, the resulting nanocomposite layer should have a large interface and continuous pathways for charge transport, due to the preformed porous structure. The copper indium disulfide layers have been prepared from solutions of the metal salts and differing amounts of thioacetamide using different temperatures up to 400 °C. The morphology and composition of the copper indium disulfide layer was investigated by x-ray diffraction, profilometer measurements, scanning electron microscopy, and atomic force microscopy.
The application of these layers for nanocomposite solar cells was not successful because of dewetting of the precursor solution on glass-ITO substrates. However, the preparation of bilayer heterojunction solar cells by applying such a layer on top of a poly(3-(ethyl-4-butanoate)thiophene-2,5-diyl] layer showed that the obtained copper indium disulfide layers are in principle well suited as acceptor material in nanocomposite photovoltaics.

KURZFASSUNG

Untersuchungen zum Schichtaufbau in Nanokomposit-Solarzellen

Im Rahmen dieser Arbeit wurden alternative Aufbaustrategien für organische und anorganisch-organische Nanokomposit-Solarzellen untersucht. Die aktive Schicht dieser Solarzellen besteht dabei entweder aus zwei organischen Halbleitermaterialien oder aus einer Kombination eines anorganischen mit einem organischen Halbleiter. Im ersten Teil der Arbeit wurden zwei verschiedene Arten der Schichtabfolge in organischen Solarzellen anhand des Donor-Akzeptor Systems Poly(3-hexylthiophen-2,5-diyl) / [6,6]-Phenyl-C_{61}-Buttersäuremethylester (P3HT/PCBM) untersucht. Die erste, derzeit gebräuchlichste, Aufbaustrategie beginnt mit der transparenten Elektrode, glasgeträgertes Indiumzinnoxid (ITO), gefolgt von einer Zwischenschicht aus Poly(3,4-ethylendioxythiophen) / Polystyrolsulfonat (PEDOT:PSS) sowie der aktive Schicht aus P3HT und PCBM und der abschließenden Aluminiumdeckelektrode. Die zweite Methode startet den Aufbau von der Aluminiumelektrode aus und schließt mit einer PEDOT:PSS Schicht, auf die eine 5 nm dünne Goldschicht aufgedampft wurde, ab.

Im zweiten Teil der Arbeit wird die Herstellung von porösen Kupferindiumdisulfidschichten für die Anwendung als anorganische Halbleiterphase in Nanokomposit-Solarzellen untersucht. Nach der Infiltrierung mit einer Polymerkomponente sollte sich eine Nanokompositschicht ausbilden, die auf Grund der bereits vorgeformten porösen Struktur sowohl eine hohe Grenzfläche als auch durchgehende Leitungspfade aufweist. Die Kupferindiumdisulfidschichten wurden aus den Lösungen der entsprechenden Metallsalze und Thioacetamid in verschiedenen Verhältnissen sowie bei verschiedenen Temperaturen bis zu 400 °C hergestellt. Die Morphologie und Zusammensetzung der Schicht wurde mittels Röntgendiffraktometrie, Profilometermessungen, Rasterkraftmikroskopie und Rasterelektronenmikroskopie untersucht. Da es im Rahmen dieser Arbeit nicht mögliche war homogene Schichten auf ITO Elektroden zu erhalten, konnten diese Schichten nicht direkt in Nanokomposit-Solarzellen untersucht werden. Es war jedoch möglich anhand eines Zweischichtaufbaus bei dem eine solche Schicht auf einer Poly[3-(ethyl-4-buttersäure)thiophen-2,5-diyl] Schicht aufgebracht wurde Solarzellen herzustellen, die zeigen, dass die hergestellten Kupferindiumsulfidschichten prinzipiell für Nanokomposit-Solarzellen geeignet wären.

ACKNOWLEDGEMENTS

I would like to thank Univ. Prof. DI Dr. Franz Stelzer, head of the Institute for Chemistry and Technology of Materials (ICTM) at Graz Technical University, and especially Univ. Doz. DI Dr. Gregor Trimmel, who was my supervising tutor, for giving me the opportunity to write this diploma thesis. Another special thank goes to DI Dr. Thomas Rath, who was somewhat like a co-supervisor to me. Thank you all for your help and support during my work! I am deeply grateful to you.

Furthermore I would like to thank all the members of this institute, in special the ones of the nanocomposite solar cells working group, for the great atmosphere, which made the work here very enjoyable and pleasant. A very special thank goes the guys of my working room, DI Dr. Eugen Maier and DI Andreas Pein, who both were also a great support for my work, and DI Lucas Hauser for their colleague- and friendship.

I also wish to thank the following persons who contributed to the content of this work: Ing. Karin Bartl for the SEM pictures, DI Sonja Larissegger for the AFM pictures and especially Stefan Moscher for the profilometer measurements and his constant support throughout my time at this institute.

Financial support of this work was provided by the project “Novel solar cell modules based on nanocomposite materials” funded by the Isovolta AG.

Last, and most of all, I wish to express my deepest gratitude to my parents, who were supporting me in a way that was unbelievable great, and especially to Susanne for motivating me in difficult times and her understanding. This would not have been possible without any of you.

TABLE OF CONTENTS

1 Introduction

1.1 World Energy Resources and Consumption

The energy consumption on earth has increased within the last 200 years as industrialisation has taken place and the world's population multiplied seven-fold. Within the 50s of the last century the automation and computing have come about and so the situation became even more dramatic. The demand for energy increased drastically over the last 60 years.

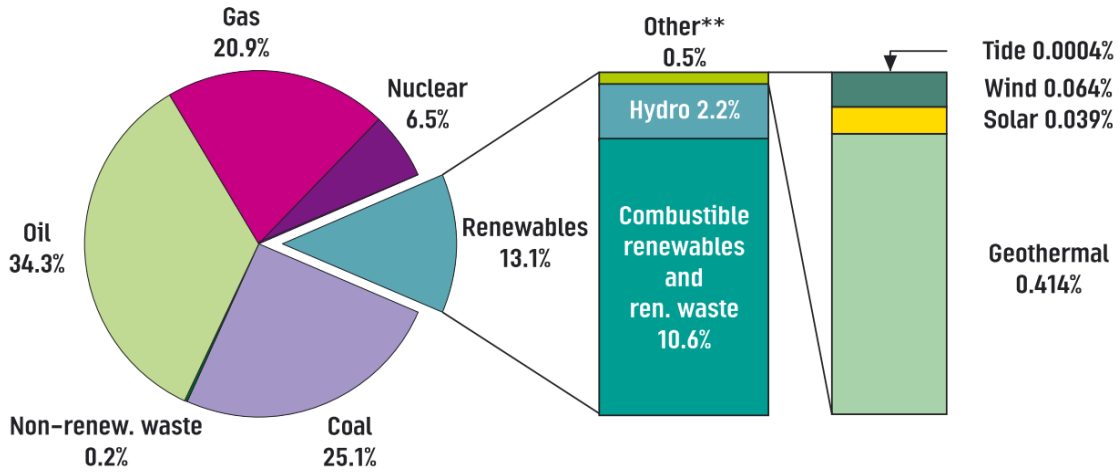

Figure 1: World energy consumption by fuel[1]

Since than fossil fuels like oil, gas and coal were used as energy sources. Just within the last decades the development of other technologies based on renewable resources such as sunlight, wind, rain, tides, and geothermal heat, is promoted by increasing public awareness that the earth's reserves on fossil fuels could run out during this century. Nevertheless still about 80% of the global energy demand is covered by fossil fuels and only 13% of the spent energy comes from renewable resources (Figure 1). If we continue to consume fossil fuels at 2006 rates, oil and gas will approximately run out in 2050 and the coal reserves will last for just another 100 years.[2] Another reason

---

1 International Energy Agency, "Renewables in Global Energy Supply", *IEA Fact Sheet* **2007**,

2 Shafiee S., Topal E., *Energy Policy* **2009**, 37, 181-189

to promote the independence of fossil fuels is the pollution that goes in hand with burning oil, gas and coal. The emerging gases like carbon dioxide have a harmful effect on the environment as they cause global warming due to the greenhouse effect. The climate problems that go along with the use of fossil energy sources might be even more serious than the danger of an energy shortage.[3] Both problems will be some of the greatest challenges in the next century, as the energy needs of the planet are likely to double within the next 50 years.[4] In order to avoid or stop global warming and cover the deficit in energy supply that will be left by fossil fuels, renewable energy has been a field of intensive research over the last 30-40 years.

1.2 Solar Energy and Organic Photovoltaics

Looking at the predicted scenario, the amount of energy needed to cover the world's demand will augment to a steady 30 terawatts per year by 2050,[3] which equals 9.5 x 10^{20} joule. It might not be possible to produce this huge amount of power only out of wind and water. This again is a point that goes in favour of solar power as the sun as energy source is nearly inexhaustible and of course sustainable. It brings an amount of about 3 x 10^{24} joules[4] per year to earth, which is about 4000 times more than the global consumption in 2050 will be. Therefore the whole need for energy could be sustained by covering about 0.2% of the earth's surface with solar cells having an efficiency of 10%.

Up to now the biggest disadvantage of solar power are the high production costs, which make electricity derived from photovoltaics about ten times more expensive than from other renewable energy technologies.[4] The solar cells that are currently present on the market are mostly based on silicon and its processing is the expensive part of the solar cell production. Therefore to reduce production costs, silicon has to be replaced by other, cheaper components.

Organic photovoltaics could be the answer. They are dealing with another principle of charge generation, which was first demonstrated by Tang in 1979[5] as he showed that an increase of power conversion efficiency could be achieved by bringing two organic

---

3 Service, R.F. *Science* **2005**, 309, 548-551

4 Grätzel M., *Nature* **2001**, 414, 338-344

5 Tang C.W., In US Patent **1979**, p 4,164,431

semiconductors into contact with each other. Furthermore, in 1986 Tang published the first organic bilayer heterojunction photovoltaic cell[6] based on this principle. These solar cells have already reached power conversion efficiencies up to 7.7%.[7]

In 1993 the first polymer/C_{60} heterojunction solar cells was prepared by Sariciftci et al.[8] and one year later Yu et al.[9] introduced the bulk heterojunction assembly using the same type of components. As these solar cells are consisting of very thin plastic layers a huge amount of solar cells could be prepared by using a very low amount of components. More than that, the used preparation techniques offer the possibility of roll to roll manufacturing, which implicates a huge reduce of the production costs as well.[3] The way of preparation leads to another advantage as the solar cells could be packaged by lamination techniques, which offers that possibility manufacturing flexible solar cells. In order to that, organic solar cells could be applied to flexible objects of everyday life like clothing[10] or bags (Figure 2).

Figure 2: Bags using polymer-based, organic photovoltaic technology to make solar power portable[11]

Due to their low production costs and their huge field of application organic solar cells and organic-inorganic hybrid solar cells, which are based on the same principles and

---

6 Tang C.W., *Applied Physics Letters* **1986**, 48, 183-185

7 Uhrich C.L., Schwartz G., Maennig B., Gnehr W.M., Sonntag S., Erfurth O., Wollrab E., Walzer K., Foerster J., Weiss A., Tsaryova O., Leo K., Riede M.K., Pfeiffer M., *Proceedings of SPIE* **2010**, 7722, 77220G/1-77220G/8

8 Sariciftci N.S., Braun D., Zhang C., Srdanov V.I., Heeger A.J., Stucky G., Wudl F., *Applied Physics Letters* **1993**, 62, 585-587

9 Yu G., Pakbaz K., Heeger A.J., *Applied Physics Letters* **1994**, 64, 3422

10 Schubert M.B., Werner J.H., *Materials Today* **2006**, 9, 42

11 http://www.konarka.com/media/pdf/konarka_casestudy_travelerschoice.pdf, accessed on 19th August 2010

have the same advantages but dealing with inorganic components as well, could become a very important technology in the future. Nevertheless, to challenge the classical energy sources on the market the three critical parameters for photovoltaics have to be optimized. Not only the costs have to be low but also the efficiency and the lifetime have to move up to get the devices ready for large-scale application.[12] If only one of the named three requirements will not be sufficiently fulfilled, organic photovoltaics will not reach such an importance on the energy market but could still be applicable for special products in niche markets. The importance of solar photovoltaic and the believe in it by the industrial sector can be determined, by the fact that it is the fastest growing power generation technology by far, with a 55% increase within one year[13] (from 2004 to 2005).

1.3 Aim of this Work

The aim of this thesis is to develop new assembly strategies for both, polymer/fullerene solar cells and nanocomposite solar cells that consist of a polymer and an inorganic layer. To be able to introduce the principle of an inverted assembly for nanocomposite solar cells a lot of preparatory investigations on inorganic layers, will be done. I will focus on $CuInS_2$ and will scrutinize the influence of the heating temperature and the amount of sulphur in the inorganic solution on the mechanical properties of the layers. Polymer/fullerene solar cells will be prepared using the common front side assembly and using a rarely investigated back side assembly. The results will be compared and discussed.

The following chapter covers the basics and theory about organic and nanocomposite solar cells and their mode of functioning. The physical principles beneath this solar cell are discussed too. Furthermore the characteristic parameters of solar cells and their practical relevance are explained as well as the state of art of this technology is highlighted. The different kinds of assembly types are explained, illustrated and discussed, especially the ones that were used during this work.

---

[12] Brabec C.J., *Solar Energy Materials & Solar Cells* **2004**, 83, 273-292

[13] Renewable Energy Policy Network for the 21th century, *Renewables - Global Status Report* **2006**

Chapter 3 contains all the results, which are discussed and illustrated. Polymer/fullerene solar cells are analyzed by the usual data and a comparison of the front and back side assembly is drawn. The investigations and experiments on the inorganic layers are discussed in detail especially the controllability of their characteristics.

In chapter 4 the experimental part of this work is described in detail. The procedures of operation are described and the used materials and equipment to do the investigations is mentioned.

A brief summary of the done work is given in chapter 5.

2 Basics

2.1 Physical Principle of Organic and Nanocomposite Solar Cells

The general process of conversion of sunlight into electric energy by an organic or nanocomposite solar cell is described to occur within six steps[14] that are described below and illustrated by Figure 3.

- Absorption of light
- Generation of excitons
- Diffusion of the excitons
- Dissociation of the excitons at the donor-acceptor interface
- Transport of the electrons towards the electrodes
- Collection of the charges at the respective electrodes

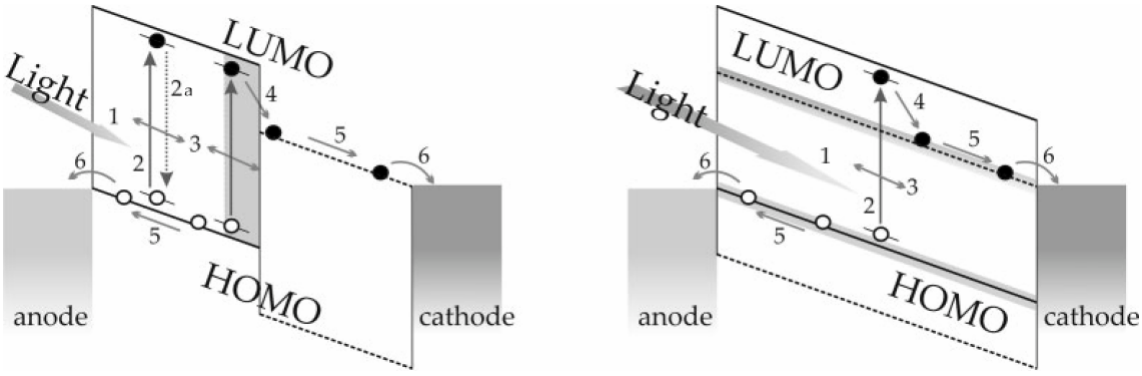

Figure 3: Schematic band diagram of the light conversion process into electric power within an organic solar cell of a (a) bilayer heterojunction and a (b) bulk heterojunction assembly[15]

[14] Nunzi J.-M., *C R. Physique* **2002**, 3, 523-542

[15] Blom P.W.M., Mihailetchi V.D., Koster L.J.A., Markov D.E., *Advanced Materials* **2007,** 19, 1551-1566

Absorption of light

The absorption is the first step in the photovoltaic power generation process. The absorption rate is determined by the optical absorption coefficient of the photoactive layer and its thickness. In polymer/fullerene solar cells the light is mainly absorbed by the polymer. Typically used polymers have a bandgap of around 2.0 eV, which implicates absorption of only 30% of the sunlight.[16] Therefore recent research direction is devoted towards the synthesis and use of low bandgap polymers[17,18] to cover a broader part of the solar spectrum. The concept of nanocomposite solar cells bases on the idea of increasing the absorption as of the photoactive layer. Inorganic semiconductors with bandgaps around the sunlight's maximum of 1.5 eV are used as acceptor material and so they contribute to the photon absorption.

The absorption rate increases with increasing photoactive layer thickness but concurrent the charge carrier and exciton mobility decreases. Hence the layer thickness is limited and so the absorption is but due to the high absorption coefficients of the used polymers 100 nm about thickness is enough to absorb most of the light in combination with a reflective back contact. Another adverse effect is the reflection loss that could be minimized by anti-reflection coatings, as they are already used in inorganic solar cells.

Generation of excitons

Within the excitation process an electron gets excited from the HOMO of the polymer to its LUMO by a photon that's energy is lower than the gap between those two orbital. This process leads to the generation of an exciton. An exciton consists of an electron and a hole paired by Coulomb energy.

Diffusion of the excitons

The generated excitons have to reach a donor-acceptor interface, where they can dissociate. The diffusion process is limited by the average length over which the exciton can diffuse within the polymer before recombination takes place. For example P3HT is said to have an exciton diffusion length of ~10 nm,[19,20] which means that

---

16 Rath T., *PhD Thesis*, **2008**, Technical University of Graz

17 Winder C., Sariciftci N.S., *Journal of Materials Chemistry* **2004**, 14, 1077-1086

18 Bundgaard E., Krebs F.C., *Solar Energy Materials & Solar Cells* **2007**, 91, 954-985

19 Saunders B.R., Turner M.L., *Advances in Colloid and Interface Science*; **2008**; 138; 1-23

20 Shaw P.E., Ruseckas A., *Samuel I.D.W., Advanced Materials* **2008**, 20, 3516-3520

excitons that are generated within the polymer phase but more than 10 nm far from the junction will recombine before getting to the interface in order to get dissociated. The recombination process leads to a annihilation of the charge carrier, as the electron and the hole combine. Although this topic is controversially discussed,[21] recombination is probably the most limiting side effect within the whole conversion process. It has been well studied[22] within the last years and thesis's to counteract have been published.[23]

Dissociation of the excitons

The steps 1 to 3 of have taken place within the polymer phase of the photoactive layer. Now, as the exciton has reached the interface between the donor (polymer) and the acceptor (fullerene, inorganic phase), exciton dissociation takes place. Here the charges, electron and hole, get separated as the electron donor keeps the hole and the acceptor takes the electron. The exciton dissociation process is in competition with luminescence and phonon emission[24] but as the dissociation process is said to happen far quicker than any competing decay process.[25,26] This step of the conversion process should be highly efficient as long as one condition is fulfilled. The donor material has to have a low ionisation potential and the acceptor material must have a high electron affinity,[26] so that equation (1) is valid.

$$E_{ex} > I_{Pd} - \chi_{Ea} \quad \textbf{(1)}$$

with

$$E_{ex} = I_{Pd} - \chi_{Ed} \quad \textbf{(2)}$$

χ_{Ea} .....electron affinity of the acceptor

I_{Pd} .....ionisation potential of the donor

χ_{Ea} .....electron affinity of the donor

E_{ex} .....exciton energy

---

[21] Deibel C., *arXiv.org, e-Print Archive, Condensed Matter* **2009**, arXiv:0907.2294v1, 1-6

[22] Wojcik M., Michalek P., Tachiya M., *Applied Physics Letters* **2010**, 96, 162102

[23] Hallermann M., Kriegel I., Como E.D., Berger J.M., von Hauff E., Feldmann J., *Advanced Functional Materials* **2009**, 19, 3662-3668

[24] Bernede J.C., *Journal of Chilean Chemical Society* **2008**, 53, 1549-1564

[25] Cook S., Katoh R., Furube A., *Journal of Physical Chemistry C* **2009**, 113, 2547-2552

[26] Peumans P., Yakimov A., Forrest S.R., *Journal of Applied Physics* **2003**, 97, 3693-3723

In words, the LUMO level of the acceptor has to be lower than the excitonic state located at the bottom of the conduction band (LUMO) of the donor, in order that a internal field, which is the driving force for charge separation, can be obtained at the donor-acceptor interface.[27]

Transport of the electrons towards the electrodes

The transport of charges is strongly related to the morphology of the photoactive phase. Continuous pathways are necessary to guarantee a high efficient charge transport towards the electrodes. Islands or dead ends, that appear especially in bulk heterojunction solar cells, lead recombination. The idea of the inverse nanocomposite solar cell assembly, which is a main part of this work, is dealing with this problem as here isolated regions should be eliminated consequently.

Furthermore a high degree of charge mobility is necessary for a high efficient charge transfer. The mobility can be reduced by traps (e.g. lattice defects).[27]

Charge collection at the respective electrodes

The charge collection, the final step of the whole process, is depends on the energy levels of the components and the interfacial contacts between the photoactive layer and the electrodes.[27] The work function of the used anode material has to be of higher energy than the HOMO of the donor and the cathodes Fermi level has to be lower than the LUMO energy level of the acceptor material.[19] At the interfaces the charge carrier often have to overcome a potential barrier of a thin oxide layer, which especially can be caused by the oxidation of the cathode material or an intentionally applied additional interfacial oxide layer.

[27] Moliton A., Nunzi J.-M., *Polymer International* **2006**, 55, 583-600

2.2 Characteristic Parameters

The I-V curves describe a photovoltaic cell concerning its electric characteristics. They are measured under dark and under illuminated conditions (Figure 4)

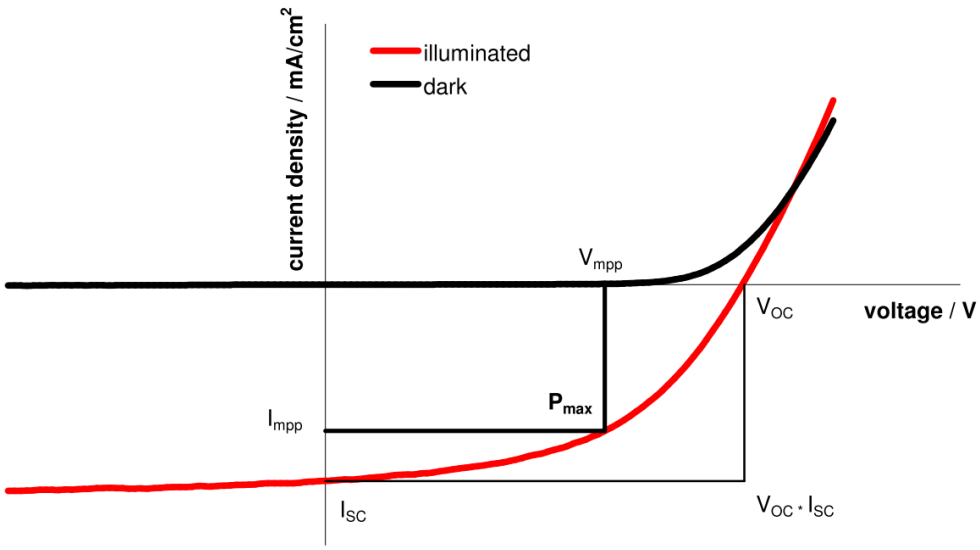

Figure 4: I-V curves of a solar cell under illuminated and dark conditions including the characteristic points.

The performance of a solar cell can be judged by the I-V curves. The curves are recorded by a source-measurement unit, as the current is measured while the voltage that is impressed on the cell runs the gamut from about 1 V to -0,5 V. The labelled points in Figure 4 are the characteristic ones of the I-V curves of each cell. The short circuit current (I_{SC}) is measured under zero applied voltage as well as the open circuit voltage (V_{oc}) is measured while the through the cell flowing current is zero. The I_{SC} is very much related to the efficiency of the in chapter 2.1 described steps of the light-to-power-conversion process. Special attention is paid to the photon absorption, the charge generation and transport. The V_{OC} is determined by the energy difference of the HOMO of the donor and the LUMO of the acceptor and by the work function of the positive electrode (e.g. ITO).[12,28] A minor dependence on the work function of the negative electrode (e.g. Al) has also been discovered.[29]

---

[28] Granqvist C.G., *Solar Energy Materials & Solar Cells* **2007**, 91, 1529-1598

[29] Brabec C.J., Cravino A., Meissner D., Sariciftci N.S., Fromherz T., Rispens M.T., Sanchez L., Hummelen J.C., *Advanced Functional Materials* **2001**, 11, 374-380

V_{mpp} and I_{mpp} are the voltage and the current density at the maximum power point, P_{max}, where the solar cell delivers the largest amount of power. As the power is determined as the product of voltage and current, at P_{max} the area of the rectangle between the axes and the curve is at its maximum. Obviously P_{max} is wished to be as high as possible and so the fill factor (FF) is an important parameter in photovoltaic science as it describes the relation between the real and the ideal power output.

$$FF = \frac{V_{mpp} * I_{mpp}}{V_{OC} * I_{SC}} \quad \textbf{(3)}$$

The fill factor is a characteristic factor for the degree of efficiency of the solar cells and is influenced by the cells serial and shunt resistance.[14]

The most important parameter to describe the performance of a solar cell is the power conversion efficiency (η_e) that names the ratio of the maximum power output to the incident light power (P_{in}).[30]

$$\eta_e = \frac{P_{\max}}{P_{in}} * 100\% = \frac{V_{OC} * I_{SC} * FF}{P_{in}} * 100\% \quad \textbf{(4)}$$

The external quantum efficiency (EQE) or incident photon to current efficiency (IPCE) describes the ratio of the external current and the incident photons. It is a experimentally accessible value and is defined in the following way:[17]

$$IPCE = EQE = \frac{\#El}{\#Ph} * 100\% = \frac{1240 * I_{SC}}{\lambda * P_{in}} * 100\% \quad \textbf{(5)}$$

The EQE can also be described as the product of the yields of the specific steps of the light-to-power-conversion process (chapter 2.1).[19]

$$EQE = \eta_A \eta_{diff} \eta_{diss} \eta_{tr} \eta_{cc} \quad \textbf{(6)}$$

η_A represents the photon absorption efficiency, η_{diss} the exciton dissociation yield, η_{diff} the exciton diffusion yield, η_{tr} the charge carrier transport yield and η_{cc} stands for the charge carrier yield.

---

[30] Nelson J., "The physics of solar cells", *London: Imperial College Press* **2003**

The standard test conditions (STC) for all kind of solar cells are 25 °C and an irradiance of 1000 W/m^2 with an air mass 1.5 spectrum. The AM 1.5 spectrum describes the spectrum of the sunlight, when it irradiates under a solar zenith angle of ~48.2° as the air mass is defined by equation (7).

$$AM = \frac{1}{\cos\theta} \quad \textbf{(7)}$$

2.3 Assembly Strategies

2.3.1 Bilayer Heterojunction vs Bulk Heterojunction

The two conventional assembly types for organic and nanocomposite solar cells are the bilayer heterojunction assembly and the bulk heterojunction assembly. The bilayer was the primarily used assembly as Tang[6] prepared the first organic solar cell in 1986 using this strategy. Seven years later the first C_{60}/polymer bilayer solar cell was prepared by Sariciftci et al.[8]. But soon the disadvantage of the bilayer was determined and the bulk heterojunction was developed as alternative assembly strategy for organic solar cells. To point out the main difference of these two strategies we have to take a deeper look at the influence the assembly could take on the performance of solar cells.

The external quantum efficiency (EQE), which is a very important parameter to describe the performance of a solar cell, is limited by the following parameters. The EQE can be described as the product of the light absorption efficiency (η_A), the exciton diffusion efficiency (η_{ED}) and the carrier collection efficiency (η_{CC}).[31] The assembly has an impact on η_{ED}, as the diffusion length of an exciton is limited to ~ 10 nm.[31,32] Hence we see the big disadvantage of the classical bilayer structure is, as the layer thickness is at least 100 nm, that not more 10% of the photogenerated excitons can only reach the donor-acceptor interface before recombining. As we can see in Figure 5 the donor-acceptor interface is much larger within the bulk heterojunction assembly, which enhances the possibility of the excitons reaching it before recombining and so increases the exciton diffusion efficiency.

---

[31] Yang X., Loos J., *Macromolecules* **2007**, 40(5), 1353-1362

[32] Saunders B.R., Turner M.L., *Advances in Colloid and Interface Science* **2008**; 138; 1-23

But as the assembly also has an influence on the carrier collection efficiency, the bulk heterojunction still offers space for advancement and further development. The η_{CC} provides information about the probability of a free charge carrier, which was generated at the donor-acceptor interface, reaching its corresponding electrode by dissociation.[31] Now the problem with the bulk heterojunction assembly is that there can be isolated parts of the donor or of the acceptor phase, which means that the generated charge carriers cannot be transferred to the electrodes.

Summarized in a bulk heterojunction solar cell the overall area of the donor-acceptor interface is much higher than it is in a bilayer, which causes an increase of the η_{ED}, but the occurrence of isolated regions cause also a decrease of the η_{CC}. Nevertheless the bulk heterojunction assembly is the much more promising one and so the more often used one since it was first published by Yu et al.[9] in 1994. To make the understanding easier a sketch of both assembly types can be seen in Figure 5.

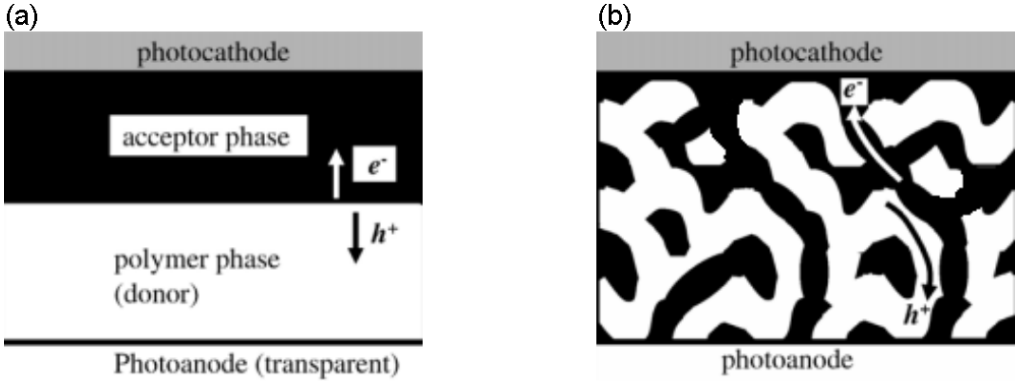

Figure 5: Schematic depiction of (a) heterojunction bilayer and (b) bulk heterojunction.[32] The bulk heterojunction has a much larger interface and much more of the polymer material is within the exciton diffusion length. On the other hand there are some isolated regions within the photoactive layer from where the charge carrier transport to the electrodes is not possible.

2.3.2 Back Side Assembled Bulk Heterojunction Solar Cells

The back side assembly for bulk heterojunction solar cells bases on the idea of cost reduction as here the ITO electrode, which is the most expensive compound within organic solar cells at the moment, is eliminated. PEDOT:PSS is used as transparent anode material instead of ITO and is applied within the last preparation step. However, sometimes a thin (3-10 nm) transparent gold layer is applied on top to enhance conductivity. So here the assembly starts with the backside of the solar cell, which is the aluminium electrode in the case of P3HT/PCBM bulk-heterojunction solar cells that

are discussed in chapter 3.1. In contrast, the common way of preparing a P3HT/PCBM bulk heterojunction solar cell is to start with the transparent ITO electrode that forms the front side of the solar cell. Therefore the ITO-free assembly is called back side assembly in the following and the common preparation technique will be named as front side assembly.

2.3.3 Inorganic-Organic Nanocomposite Solar Cells

Alternatively, organic-inorganic hybrid materials consisting of an organic donor and a nanostructured inorganic acceptor can be used as active layer in plastic photovoltaic.[19,33,34] This assembly allows an almost infinite number of combinations of inorganic and organic semiconductors. Using inorganic nanostructures offers the possibility of the use of a multitude of different shapes of the semiconductor, for example spherical, rod-like, rectangular, nanoparticles (Figure 6), and branched crystals. Furthermore the size of the structures is a tuneable parameter due to quantum confinement effects[35]. Already realized combinations of blends of a conjugated polymer and nanocrystals are for example CdSe[36,37,38,39], CdS[40], ZnO[41,42], $Zn_{1-x}Mg_xO$[43], CdTe[44,45], InAs[46], $CuInS_2$[47], $CuInSe_2$[48], PbS[49,50], PbSe[51], or TiO_2[52,53,54]. Power

---

33 McGehee M.D., *MRS Bulletin* **2009**, 34, 95-100

34 Holder E., Tessler N., Rogach A.L., *Journal of Materials Chemistry* **2008**, 18, 1064-1078

35 Talapin D.V., Lee J., Kovalenko M.V., Shevchenko E.V., *Chem. Rev.* **2010**, 110, 389-458

36 Huynh W.U., Dittmer J.J., Libby W.C., Whiting G.L., Alivisatos A.P., *Advanced Functional Materials* **2003**, 13, 73-79

37 Sun B., Greenham N.C., *Physical Chemistry Chemical Physics* **2006**, 8, 3557-3560

38 Sun B., Snaith H.J., Dhoot A.S., Westenhoff S., Greenham N.C., *Journal of Applied Physics* **2004**, 97, 014914

39 Albero J., Martinez-Ferrero E., Ajuria J., Waldauf C., Pacios R., Palomares E., *Physical Chemistry Chemical Physics* 2009, 11, 9644-9647

40 Greenham N.C., Peng X., Alivisatos A.P., *Physical Review B* **1996**, 54, 17628

41 Beek W.J.E., Wienk M.M., Janssen R.A.J., *Advanced Materials* **2004**, 16, 1009-1013

42 Ravirajan P., Peiro A.M., Nazeeruddin M.K., Graetzel M., Bradley D.D.C., Durrant J.R., Nelson J., *Journal of Physical Chemistry B* **2006**, 110, 7635-7639

43 Olson D.C., Shaheen S.E., White M.S., Mitchell W.J., vanHest M.F.A.M., Collins R.T., Ginley D.S., *Advanced Functional Materials* **2007**, 17, 264-269

44 Kumar S., Nann T., *Journal of Materials Research* **2004**, 19, 1990-1994

45 Gur I., Fromer N.A., Alivisatos A.P., *Journal of Physical Chemistry B* **2006**, 110, 25543-25546

46 Anctil A., Landi B., Worman J., Raffaelle R., *Materials Research Society Symposium Proceedings* **2007**, 1013, Z07-30

47 Piber M., Rath T., Griesser T., Trimmel G., Stelzer F., Meissner D., *Conference Record of the 2006 IEEE 4th World Conference on Photovoltaic Energy Conversion* 2006, 1, 247

conversion efficiencies of hybrid plastic solar cells are still low compared to fullerene based devices reaching efficiencies within the range of 2.5 %[19] to 3.13 %[55], which was reached recently by using CdSe-nanostructures. Beside the most researched polymer/ assembly types some other strategies to prepare nanocomposite solar cells, such as nanoparticles mixed with conducting and semiconducting polymers (Figure 6). Such solar cells were produced using $CuInS_2$-nanoparticles[56,57] and CuInSe-nanoparticles,[58,] for instance.

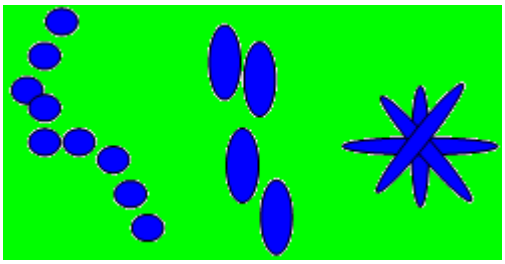

Figure 6: Nanoparticles of inorganic compounds mixed with a polymer

Some of the inorganic semiconductor materials (e.g. ZnO) can be prepared in a highly ordered fashion, e.g. in nanorod arrays that are highly ordered nanosized channel structures (Figure 7),[59,60] and have recently been investigated in this type of solar cells.

---

[48] Arici E., Hoppe H., Schäffler F., Meissner D., Malik M.A., Sariciftci N.S., *Thin Solid Films* **2004**, 451-452, 612-618

[49] McDonald S.A., Konstantatos G., Zhang S., Car P., Klem E.J.D., Levina L., Sargent E.H., *Nature Materials* 2005, 4, 138-142

[50] Günes S., Fritz K.P., Neugebauer H., Sariciftci N.S., Kumar S., Scholes G.D., *Solar Energy Materials & Solar Cells* **2007**, 91, 420-423

[51] Jiang X., Schaller R.D., Lee S.B., Pietryga J.M., Klimov V.I., Zakhidov A.A., *Journal of Materials Research* **2007**, 22, 2204

[52] Salafsky J.S., *Physical Review B: Condensed Matter and Materials Physics* **1999**, 59, 10885-10894

[53] Boucle J., Ravirajan P., Nelson J., *Journal of Materials Chemistry* **2007**, 14, 3141-3153

[54] Zeng T., Lo H., Chang C., Chen Y.L.a.C., Su W., *Solar Energy Materials & Solar Cells* **2009**, 93, 952-957

[55] Dayal S., Kopidakis N., Olson D.C., Ginley D.S., Rumbles G., *Nano Letters* **2010**, 10, 239

[56] Arici E., Sariciftci N.S., Meissner D., *Advanced Functional Materials* **2003**, 13, 165-171

[57] Arici E., Sariciftci N.S., Meissner D., *Molecular Crystals and Liquid Crystals* **2002**, 385, 129-136

[58] Arici E., Hoppe H., Schäffler F., Meissner D., Malik M.A., Sariciftci N.S., *Applied Physics A* **2004**, 79, 59-64

[59] Salafsky J.S., *Solid-State Electronics* **2001**, 45, 53-58

[60] Kannan B., Castelino K., Majumdar A., *Nano Letters* **2003**, 3, 1729-1733

In this approach the nanostructures are prepared in a first step and the organic component is applied afterwards in a separate infiltration step.

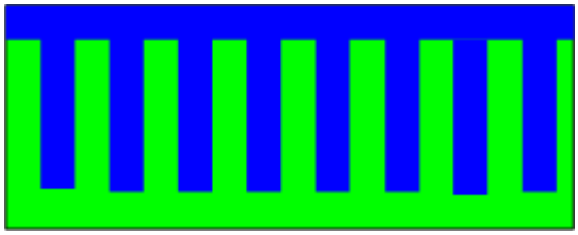

Figure 7: Highly ordered structure of the inorganic compound that can be reached by applying different imprint techniques.

2.3.4 Inverse Assembled Nanocomposite Solar Cells

The idea of the above mentioned nanorod arrays is to eliminate the disadvantages of the common used techniques, the bilayer and the bulk heterojunction solar cells, as a large interface as well as continuous pathways for the charges are realized. This concept is also followed in the herein investigated inverse assembled nanocomposite solar cells using $CuInS_2$ as acceptor material. This should be possible by preparing a highly porous $CuInS_2$ layer first, which will eliminate isolated inorganic areas as the porous structure of this inorganic layer might be controllable by its chemical composition and the thermal treatment. As the polymer is only applied within the next preparation step, it is possible to anneal the $CuInS_2$ layer at higher temperatures, which might lead to the desired layer morphology. The goal is to reach an intrinsic structured inorganic layer so that the solution of the conjugated polymer, which would be applied next, can diffuse into the resulting cavities. Hence it should be possible to get a structured assembly of the photoactive layer with a large interface and no isolated regions. However, this means, that from the theoretical point, the commonly layer ordering ITO-polymer-$CuInS_2$-Al has to be inverted and the inorganic part (acceptor) will be put about the ITO which should act as cathode in this assembly. Because of the changed layer order and the consequential changed energy levels of the solar cell, adjustments of the anode have to be done as other materials than aluminium, for instance gold, have to be used.

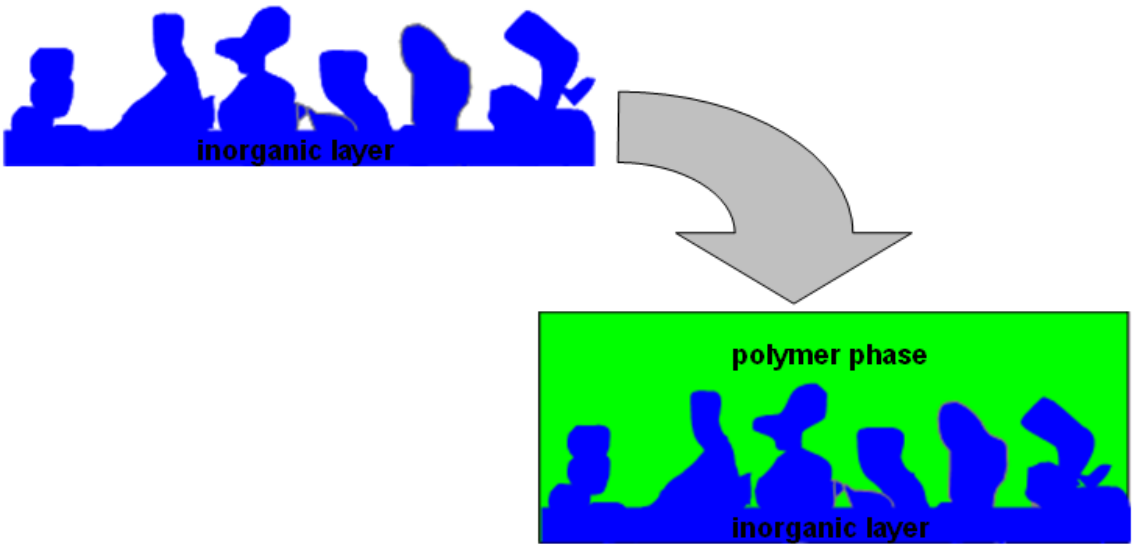

Figure 8: **Inorganic nanostructured layer infiltrated by a polymer leading to a photoactive layer with a large donor-acceptor interface and without dead ends.**

3 Results and Discussion

3.1 Polymer Fullerene Solar Cells

The well studied and known system of the P3HT/PCBM solar cells was chosen to prepare solar cells with the common front side bulk heterojunction architecture and solar cells with the back side bulk heterojunction architecture. The idea of the back side assembly is to reduce production costs by eliminating the ITO electrode, which is the most expensive organic solar cell compound at the moment.

3.1.1 Front Side Assembly

As this kind of solar cells are polymer/fullerene bulk heterojunction solar cells. This means that their photoactive layer consists of a conjugated polymer (P3HT) and a fullerene (PCBM), that are mixed together to a mutual solution, a so called bulk, before being applied. Solar cells of such an assembly have already reached power conversion efficiencies of up to 3.4%[61] using chloroform and up to 5%[62,63] by using chlorobenzene as solvent. Rather recently Liang et al published a PCE of even 7.4%.[64] The reason for this significant difference is manifested by the better solubility of PCBM in chlorobenzene and the hence resulting better crystal packing in the films coated out of chlorobenzene.[65] Nevertheless here chloroform was the solvent of choice due to its lower toxicity compared to chlorobenzene. Furthermore ITO-covered glass substrates that were etched by using HCl and zinc powder as described in chapter 4.2.1 were used to avoid short circuits. The first applied film was PEDOT:PSS, poly(ethylene-dioxythiophene) doped with polystyrenesulfonic acid, which was coated on the etched ITO-substrate and acts as the photoanode of the solar cell in combination with the ITO

---

[61] Al-Ibrahim M., Ambacher O., Sensfuss S., Gobsch G., *Applied Physics Letters* **2005**, 86, 201120

[62] Ma W., Yang C., Gong X., Lee K., Heeger A.J., *Advanced Functional Materials* **2005**, 15, 16

[63] Lee K., Kim J.Y., Heeger A.J., *Proc of SPIE* **2006**, 6117, 61170T.

[64] Liang Y.Y., Xu Z., Xia J.B., Tsai S.-T., Wu Y., Li G., Ray C., Yu L.P., *Advanced Materials* **2010**, 22, E135-E138

[65] Rispens M.T., Meetsma R., Rittberger R., Brabec C.J., Sariciftci N.S., Hummelen J.C., *Chemical Communication* **2003**, 17, 2116.

layer. Afterwards a layer of the photoactive bulk was applied followed by the aluminium electrode, which was put about by vacuum evaporation through a mask. The mask was used to get a defined area of the electrode to ensure the correctness of the calculation of the efficiency during the analysis. Summarized the solar cells had the following configuration: glass / ITO / PEDOT:PSS / (P3HT/PCBM) / Al. This assembly of such a polymer solar cell is shown schematically in Figure 9. An area of about 3 to 4 millimetres of the ITO layer is uncovered at the not etched end of the device in order to be able to contact the electrode with the measurement tip to record the I-V curves.

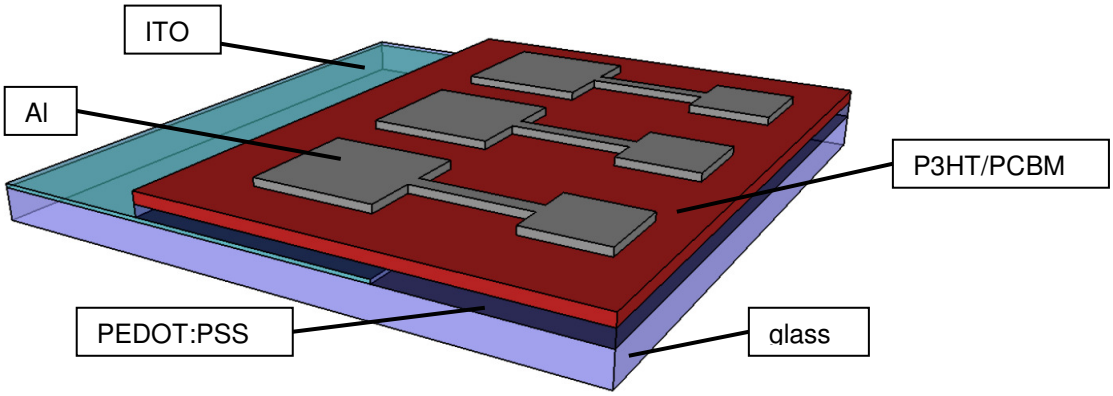

Figure 9: Assembly of a P3HT/PCBM bulk heterojunction solar cell with the common architecture

3.1.2 Back Side Assembly

Using the common architecture we start the construction of the solar cell with the photoanode, ITO in this case, which is the transparent electrode and forms the top of the solar cell. It is placed on a transparent substrate, glass in most times. Now by using the back side structure we start at the other end of the solar cell, at the photocathode. Glass was chosen as substrate because of practical reasons, as the applicable pre-treatment, which is a crucial step in the whole solar cell preparation process, and its wetting characteristics are already known quite well. Here aluminium was used as cathode again, but beforehand a thin titanium layer of roughly 5 nm was applied onto the substrate to improve the adhesion of aluminium to it.[66] After the evaporation of the aluminium layer (~200 nm) again a thin layer of ~3 nm was applied, but this time to avoid passivation of the electrode that could happen easily to aluminium by the

[66] Zimmermann B., Glatthaar M., Niggemann M., Riede M.K., Hinsch A., Gombert A., *Solar Energy Materials & Solar Cells* **2007**, 91, 374-378

oxidation through atmospheric oxygen. All the metals were applied by vacuum evaporation. Then the photoactive bulk (P3HT/PCBM) was applied by spin coating as well as the following layer of PEDOT:PSS. The last step was to apply the second component of the transparent electrode, which was gold in this case. A thin layer of 10 nm was brought up by vacuum evaporation through a mask to get a defined electrode area. So this kind of solar cells had the following configuration: glass / Ti / Al / Ti / (P3HT/PCBM) / PEDOT:PSS / Au. A back side assembled bulk heterojunction solar cell is shown in Figure 10 and again an area of about 3 to 4 millimetres of the lower electrode, which is aluminium in this case, is uncovered. Furthermore the aluminium electrode is not put about the entire substrate. An area of about 3 millimetres length was kept blank during the aluminium evaporation process in order to avoid short circuits during the I-V measurements.

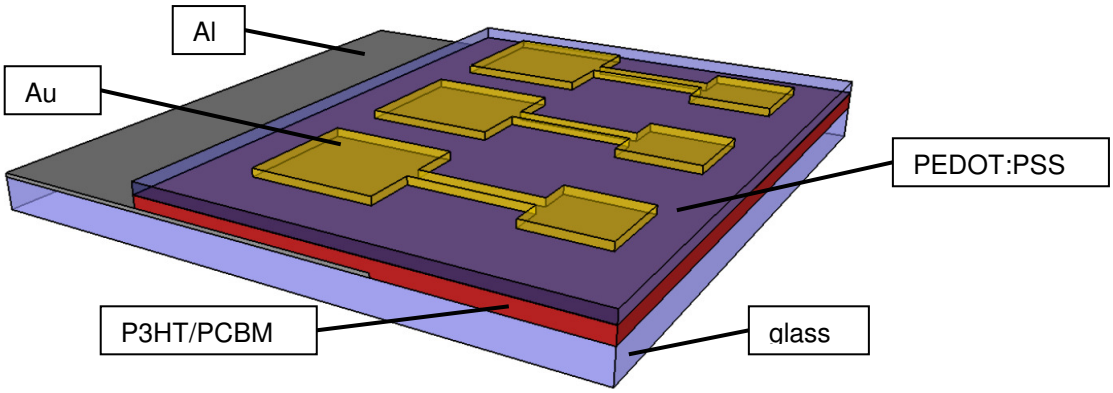

Figure 10: Assembly of a P3HT/PCBM bulk heterojunction solar cell using the back side architecture

3.1.3 Mode of Operation in P3HT/PCBM Solar Cells

P3HT is a light harvesting polymer with a reported[67] absorption maximum at 2.48 eV equally to a wavelength of 500 nm. As the sunlight has its highest intensity in the same range, P3HT is a suitable absorber. The Bandgap of P3HT is reported to be within the range of 1.9 eV[67,68] to 2.1 eV[69] most of the time but also a bandgap of just 1.7 has been published already.[70] UV-Vis measurements (Figure 11) in order to determine the absorption maximum and the bandgap of the P3HT were done as well as CV measurements to get further information for the bandgap determination. The UV-Vis measurements showed an absorption maximum at 530 nm and an onset between 720 and 735 nm, equally to 1.69 to 1.72 eV. CV measurements showed a Bandgap of 1.72. Although these measurements lead to slightly higher wavelength concerning both, absorption maximum and bandgap, the results go along with reported data in literature quite well. One reason for the slightly differing data concerning the optical properties of P3HT might be the degree of regioregularity of the used polymers. The regioregularity on the polymer main chain is quite an important factor for characteristics such as conductivity and charge mobility of the polymer and hence has great influence on the device performance of solar cells.[18] In this case being at the lower edge concerning the bandgap of the polymer (1.72 eV) might be positive due to the fact that the “ideal polymer” for bulk heterojunction solar cells should have a bandgap of about 1.5 eV, keeping the solar spectrum in mind. As the sunlight has its absorption maximum at 500 nm or a little above, P3HT is a very well chosen polymer for the preparation of organic solar cells. Figure 11 shows the UV-Vis spectrum of P3HT in comparison to the AM 1.5 spectrum.

---

[67] Al-Ibrahim M., Sensfuss S., Uziel J., Ecke G., Ambacher O., *Solar Energy Materials & Solar Cells* **2005**, 85, 277-283

[68] Mühlbacher D, Scharber M., Morana M., Zhu Z., Waller D., Gaudiana R., Brabec C., *Advanced Materials* **2006**, 18, 2884-2889

[69] Koster L.J.A., Mihailetchi V.D., Blom P.W.M., *Applied Physics Letters* **2006**, 88, 093511

[70] Al-Ibrahim M., Roth H.-K., Zhokavets U., Gobsch G., Sensfuss S., *Solar Energy Materials & Solar Cells* **2005**, 85, 13-20

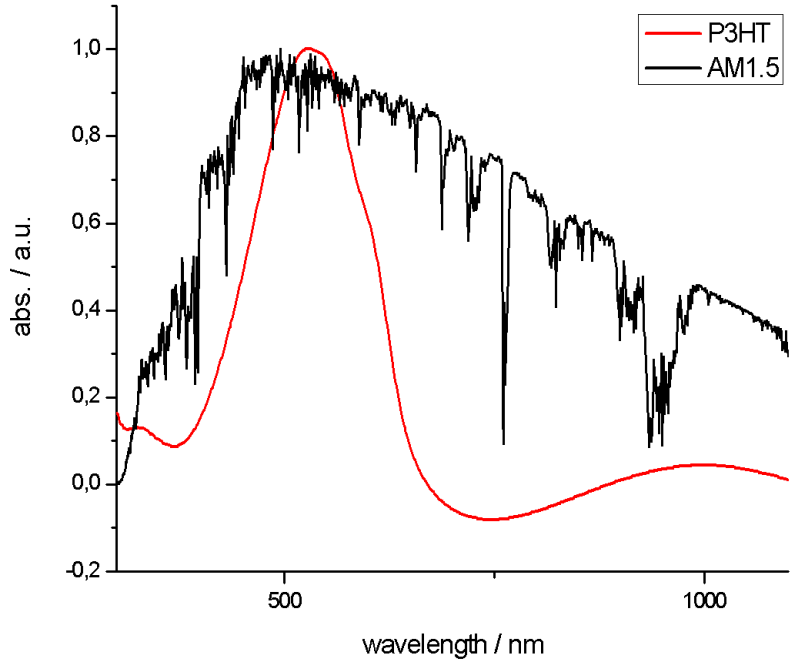

Figure 11: UV-Vis spectrum of the used P3HT (red) showing an absorption maximum of 530 nm and an onset of about 720 nm, which means a bandgap of 1.72 eV. The black line shows the AM1.5 spectrum of the sun with its maximum around 500 nm.

As this kind of solar cell is belonging to the group of donor-acceptor solar cells with P3HT being the donor and PCBM being the acceptor, the charge generation works as follows. Under illumination photons are absorbed by P3HT, the conjugated polymer, initiating the excitation of electrons from the donors HOMO to its LUMO. The bound electron-hole pair is separated at the P3HT-PCBM interface which leads to an electron in the LUMO of PCBM (acceptor) and an hole in the HOMO of P3HT (donor). Now the electrons are transferred to aluminium, the photocathode, and the holes get to the photoanode, ITO in this case. The energy levels of P3HT/PCBM solar cells are shown in Figure 12.

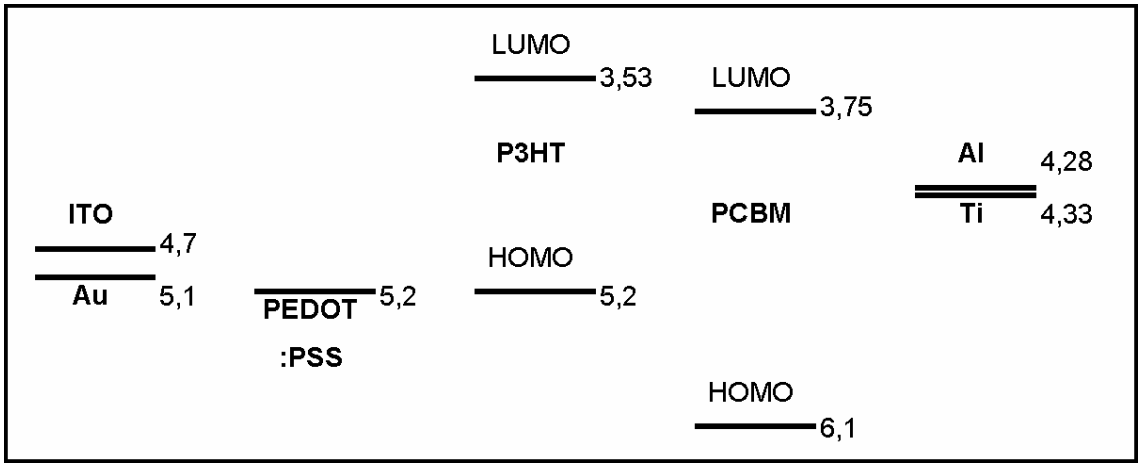

Figure 12: Energy-level diagram showing the HOMO and LUMO energies of each of the component materials as well as the work functions of the used electrode materials.

The difference of the work functions of the two anode materials, gold and ITO, does not really matter, because PEDOT:PSS has a considerable influence, which means, that it has the functionality of the photoanode in some way. It is placed directly next to the photoactive layer and so the holes are attracted by PEDOT:PSS before they get to the ITO (common, front side assembly) or gold (back side assembly) electrode. At the back side assembly we have to mention that the presence of the titanium layer between the photoactive layer and the cathode has an effect on the work function of the photocathode as the titanium might shift the electrodes energy level. The thin titanium layer between aluminium and PCBM avoids the formation of aluminium oxides that would implicate a passivation of the electrode, as already mentioned. Instead of that here titanium is oxidized by atmospheric oxygen itself. But as the titanium layer has a thickness of just 3 nm the titanium oxide film is much thinner than the oxide film of the more reactive aluminium would be. Therefore the influence of the titanium oxide film, which has a thickness of approximately 2-3 nm, was neglected. Due to its low thickness of less than 5 nm and the fact that its work function is just 0.05 eV higher than the one of aluminium the influence of the non oxidized titanium layer on the electrodes overall behaviour was neglected as well.

3.1.4 I-V Curves

The solar cells were prepared in both architectures and I-V measurements were recorded. Right at the beginning both types showed a rather bad performance, with low short circuit currents between 0.1 and 0.4 mA/cm^2 and surprisingly bad fill factors of only that were in the range of 12 to 20 %. As a result only low values of PCE have been achieved. They were between 0.1 and 0.35 %. The I-V curve of such a bulk heterojunction solar cell, prepared using the common assembly, can be seen in Figure 13.

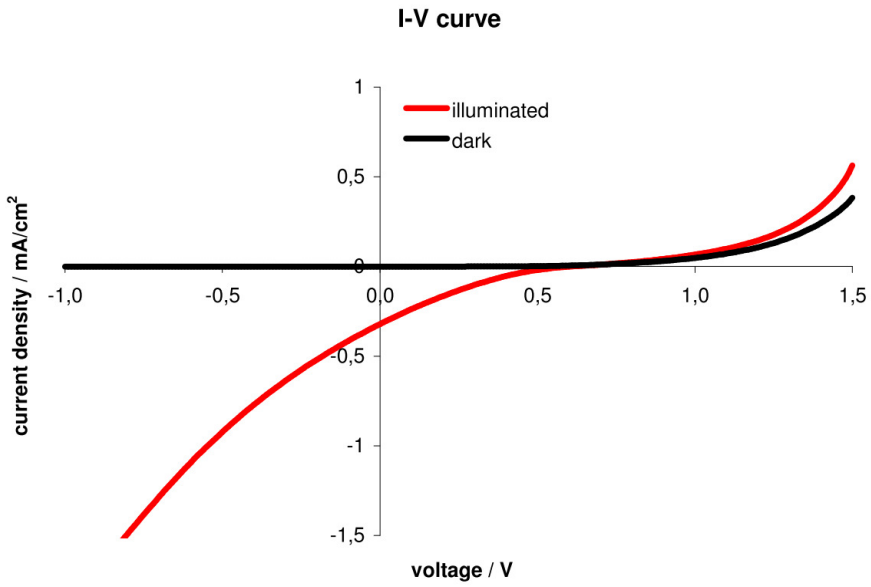

Figure 13: I-V curve of a common prepared BHJ solar cell with low I_{SC} and bad FF

3.1.4.1 Front Side Assembly

Within the following experiments it was tried to eliminate the cause of defect. The used solvent turned out to be the error source. Therefore new and fresh chloroform of a purity of more than 99.999% was used and so the performance of the solar cells improved. In order to that a P3HT/PCBM solar cell that reached a short circuit current density (I_{SC}) of 11.3 mA/cm^2, an open circuit voltage (V_{OC}) of 660 mV, a fill factor (FF) of 49.8% and an overall efficiency (η) of 3.70% was prepared. The I-V curve of this common prepared solar cell is shown in Figure 14.

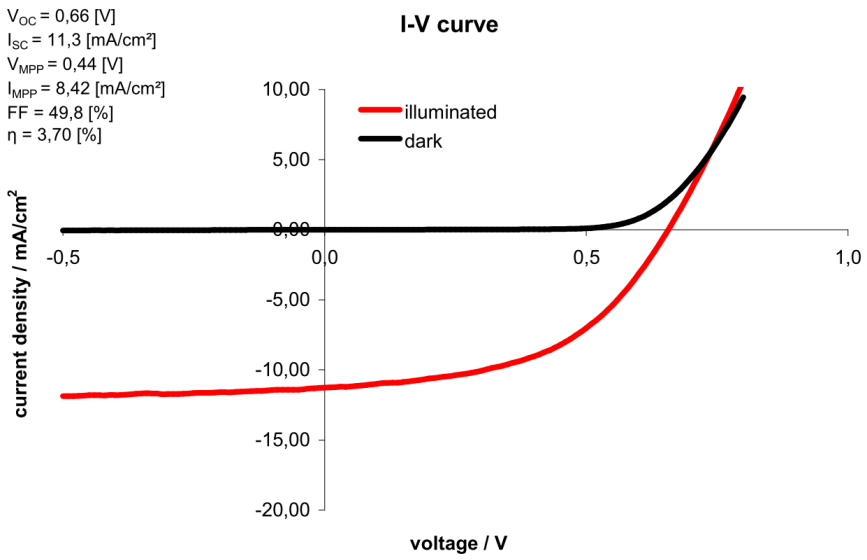

Figure 14: I-V curve of a common prepared BHJ solar cell with its analysis values.

Al-Ibrahim[61] et al. got to similar characteristic values using the common way of preparation resulting in an overall efficiency of 3.4%. So this data belong to the highest PCE ever reached under atmospheric oxygen and using chloroform as solvent.

3.1.4.2 Back Side Assembly

The best back side assembled solar cell, shown in Figure 15, had a short circuit current of 11.55 mA/cm^2, an open circuit voltage of 600 mV, a fill factor of 31.4% and an overall efficiency of 2.18%.

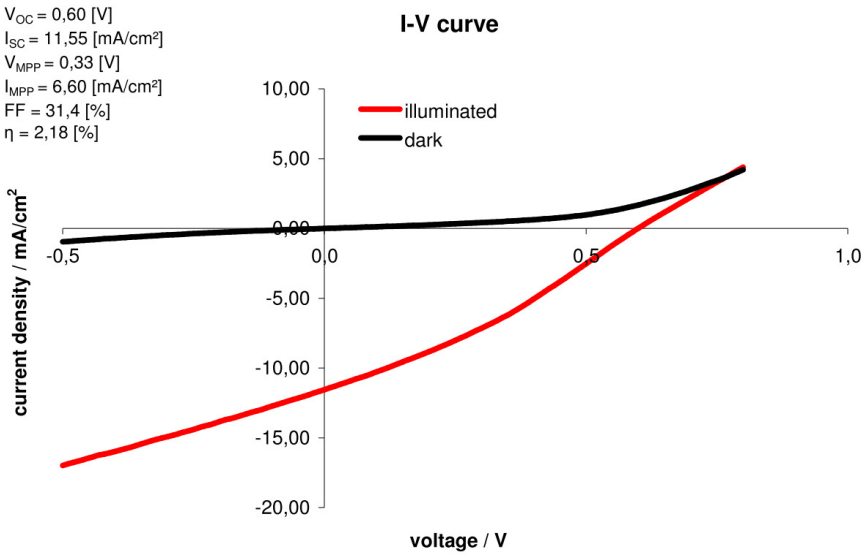

Figure 15: I-V curve of an back side assembled BHJ solar cell with its analysis values. Beside the good I_{SC} and V_{OC} values the bad fill factor stands out.

3.1.5 Comparison of Assemblies

3.1.5.1 I-V Characteristics

Table 1: Comparison of the characteristic data of the two different assemblies

Assembly	V_{OC} / mV	I_{SC} / mA/cm^2	FF / %	η / %
common	660	11.3	49.8	3.70
back side	600	11.55	31.4	2.18

As we can see the V_{OC} of the back side assembled solar cell is a little lower and the I_{SC} is a little higher, nearly the same, but the fill factor is much lower than the one of the common prepared solar cell. As the same donor and acceptor materials were used in both cells, which were prepared under the same conditions, the reason for significant difference of a nearly 40% lower fill factor could not be determined yet. It might be by the virtue of differences in the morphology of the photoactive layer or the electronic properties at the contact/polymer interface.[67] The first assumption seems to be more unlikely, since the composition of the photoactive layer is the same at both assemblies, as already mentioned. Probably the latter explanation is a better one in this case, due to the fact that for the two different assembled types of solar cells, different PEDOT:PSS solution had to be used due to wetting reasons. Furthermore we have to consider that as a result of the changed order of the preparation steps the timeframe between the application and the annealing of the PEDOT:PSS layer changed significantly. The PEDOT:PSS layer was annealed immediately after being applied at the front side assembly. At the back side assembly it was transferred to the evaporation unit and partially covered with gold there before the annealing step took place. This time shift of about 3 hours might have an influence on the charge transfer at the contact/polymer interface. Anyway further investigations are necessary to proof this assumption.

A high degree of reproducibility was reached within the last prepared type series. In Figure 16 the efficiencies of all front side and back side solar cells that have been prepared within the last three type series are plotted. The first series was prepared by using a bulk solution in chloroform containing 10 mg PCBM and 8 mg P3HT, which is said to be the best ratio. The last two ones were prepared by using a solution with a slightly higher ratio of P3HT of about 8.3 mg, which turned out to lead to even better

results. Furthermore the first type series shown in Figure 16 was prepared with a chloroform puriss. p.a. and not with chloroform CHROMASOLV ≥ 99.999%, as the latter ones were. The figure also shows that the performance of the solar cells got better with each series. This might be due to the preparation that got better with time as I got more and more used to the preparation techniques.

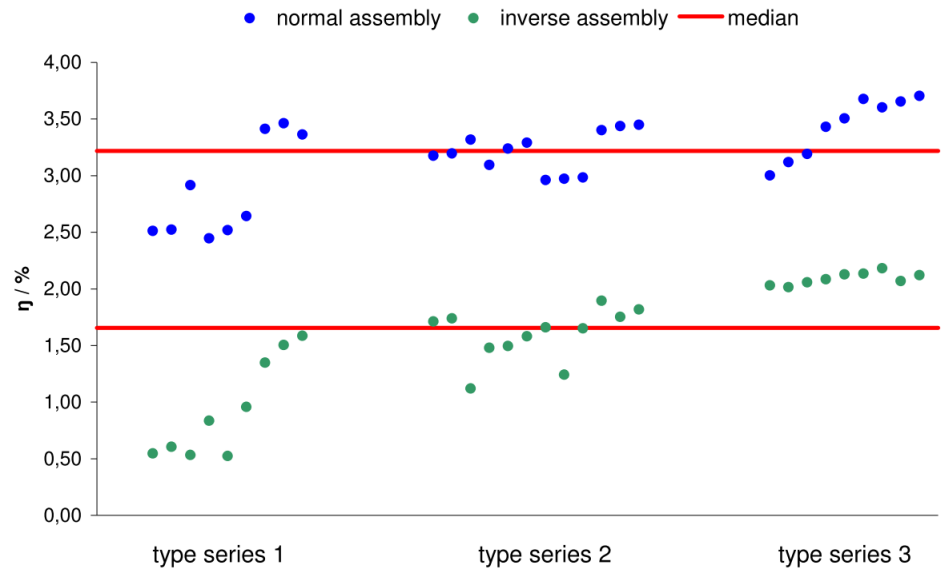

Figure 16: Achieved efficiencies within the last three type series' of front side (blue) and back side (green) solar cells. The median is marked in both cases by a red line.

We can see that the Median of the efficiency of the common assembled solar cells is at 3.22% and the one of the back side assembled solar cells at 1.66%. Within the last type series even better results could be achieved. All the back side assembled cells of the last type series showed efficiencies between 2.01 and 2.14% and looking at the last series of front side assembled cells it seems to be possible to prepare solar cells of this type showing efficiencies of more than 3.5% in a reproducible way.

3.1.5.2 Layer Thickness

The two different assemblies were analyzed concerning the thickness of the single layers of the solar cell. For the ITO-covered devices that were used to prepare the front side assembled cells the first applied PEDOT:PSS layer (Figure 18) and the photoactive layer (Figure 19) were measured. The ITO layer thickness was also measured and determined to be around 185 nm and showing a very flat surface (Figure 17).

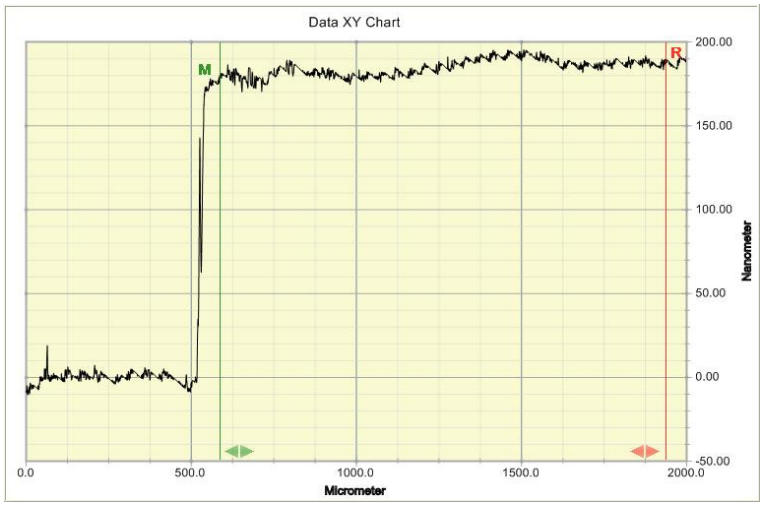

Figure 17: Profilometer measurements of the ITO layer on the used devices

As the adhesion properties and wetting conditions of the different compounds have a significant influence on the layer thickness the measurements of the layers were done by a cumulative method. That means that the samples where prepared as they were within the front side assembled solar cell preparation but the process was stopped after the respective layer was applied. The annealing steps were included.

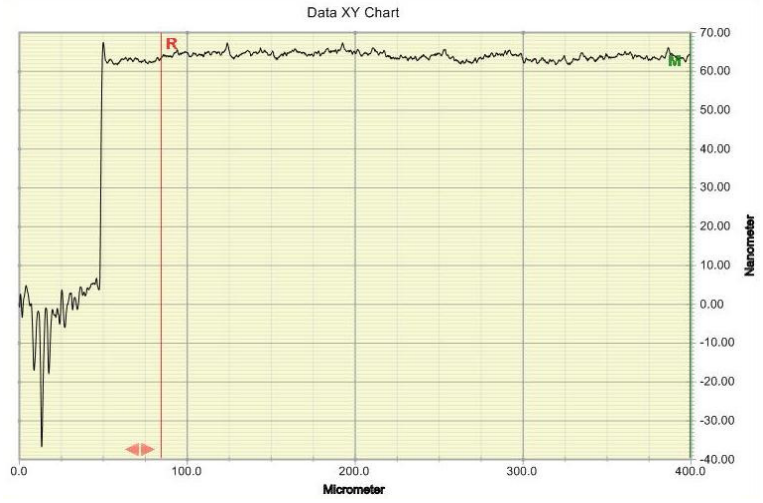

Figure 18: Profilometer measurements of the PEDOT:PSS layer (front side assembly)

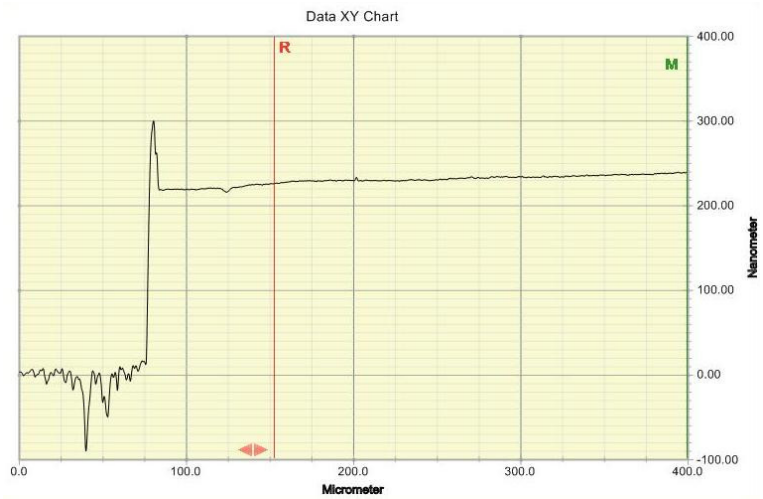

Figure 19: Profilometer measurements of the photoactive and the PEDOT:PSS layer (front side assembly)

For the backside assembly the PEDOT:PSS layer (Figure 22), the P3HT/PCBM layer (Figure 21) and the Ti-Al-Ti electrode (Figure 20), which was applied by vacuum evaporation as first, were measured. The profilometer measurements of the electrode go along with the one of the oscillating quartz crystal of the evaporation unit, where a layer thickness of 5 nm titanium, 200 nm aluminium and 3 nm titanium was programmed.

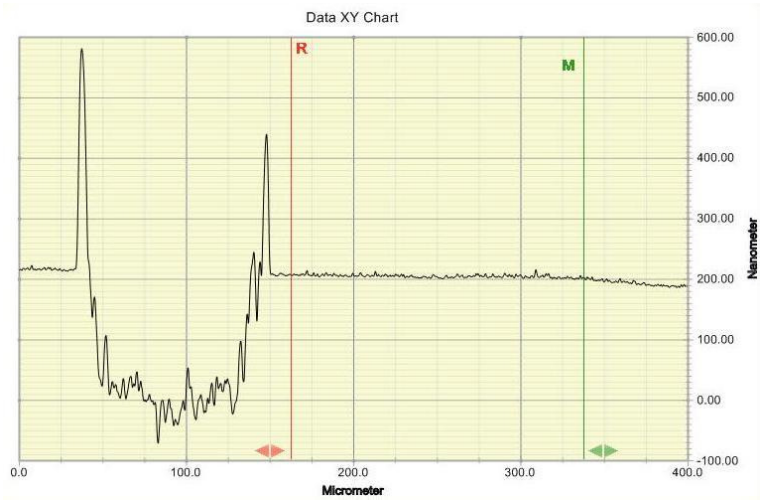

Figure 20: Profilometer measurements of the Ti-Al-Ti electrode (back side assembly)

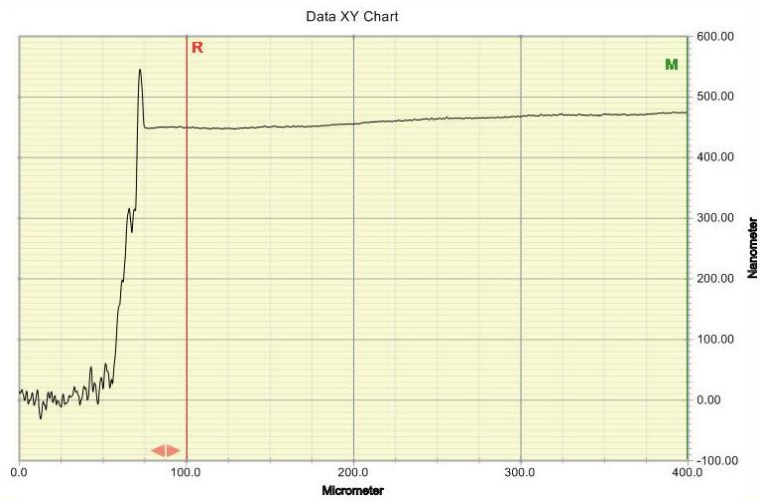

Figure 21: Profilometer measurements of the cumulated thickness of the photoactive layer and the Ti-Al-Ti electrode (back side assembly)

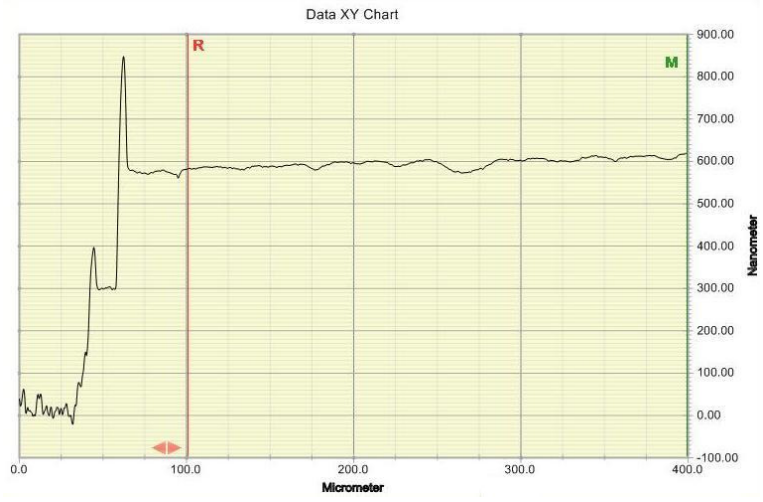

Figure 22: Profilometer measurements of the cumulated thickness of the PEDOT:PSS layer, the photoactive layer and the Ti-Al-Ti electrode (back side assembly)

The thickness of the PEDOT:PSS layer is about 65 nm at the front side assembled solar cell and about 120 nm using the backside assembly. As the same spin coating parameter were used at both techniques, this effect might be based on the difference of the PEDOT:PSS solutions that had to be used due to completely different wetting conditions on ITO and the PCBM/P3HT layer.

The photoactive layer is also thicker at the back side assembled solar cell than it is within the front side assembly, showing a thickness of 260 to 270 nm compared to about 180 nm. In this case the differing electrode materials and the wetting conditions of the bulk solution on them are the only possible explanation for this significant

difference. On the one hand thicker films absorb more photons but on the other hand their morphological organisation is worse due to a lower crystallinity of P3HT, especially next to the photoanode.[71] Furthermore an increase of the photoactive layer thickness leads to a decrease of the charge mobility and therefore to a decrease of the current density. Overall the layer thickness is reported[72] to have no great influence on the performance of P3HT/PCBM solar cells. Especially as the mainly noticed effect is a decrease of the short circuit current density,[72,73] and not a decreasing fill factor, which is the case for the back side assembled solar cells here, the high photoactive layer thickness might not be the reason for their worse performance.

Nevertheless the layer thicknesses that were reached with the front side assembled solar cells are in a range witch are said to be the best. A PEDOT:PSS layer thickness of around 70 nm[72,74] and a P3HT/PCBM layer thickness within the range of 160 to 220 nm[73] are reported to lead the highest efficiencies. Therefore a reduction of the P3HT/PCBM layer thickness that can be easily reached by an increasing spin coating rate or reducing the concentrations in the coating solutions, might lead to a better performance of the back side assembled solar cells.

---

[71] van Bavel S., Sourty E., de With G., Frolic K., Loos J., *Macromolecules* **2009**, 42, 7396-7403

[72] Kim Y., Ballantyne A.M., Nelson J., Bradley D.D.C., *Organic Electronics* **2009**, 10, 205-209

[73] Hui J., Olkkonen J., Tuomikoski M., Kopola P., Maaninen A., Hast J., *Solar Energy Materials & Solar* Cells **2010**, 94, 465-470

[74] Friedel B., Keivanidis P.E., Brenner T.J.K., Abrusci A., McNeill C.R., Friend R.H:, Greenham N.C., *Macromolecules* **2009**, 42, 6741-6747

3.2 Inorganic layers

The second part of this work deals with the preparation $CuInS_2$ layers. This types of inorganic layers were prepared because of their electronic and optical properties that make them applicable as acceptor material within hybrid solar cells. They were investigated on their usability as inorganic layer for nanocomposite solar cells and for inverse nanocomposite solar cells in special. Furthermore, experiments on their structure were done and it was tried to find out preparation techniques that enable to take influence on the layer characteristics concerning their morphology.

Based on the idea of building an inverse nanocomposite solar cell the $CuInS_2$ layers were prepared on ITO-covered glass substrates. As described in chapter 4.5 for the X-ray diffraction and UV-Vis measurements the layers were prepared out of solutions with differing amount of sulphur. Solutions with a sulphur excess of 1.2, 5 and 10 were prepared, layers were prepared by spin coating and one sample of each solution was annealed at 200°C, 300°C and 400°C. These experiments were done to investigate the optical properties, the porosity and the degree of crystallinity of the $CuInS_2$ layers and the effect of the higher annealing temperatures on these layer properties. As at the common assembly the inorganic layer is applied after the polymer, its annealing temperature is strongly limited by the polymers sensitivity to the heat (~180°C). Using the inverse assembly, this limiting factor is eliminated and so it is possible to anneal the $CuInS_2$ layer at such high temperatures.

3.2.1 UV-Vis Measurements

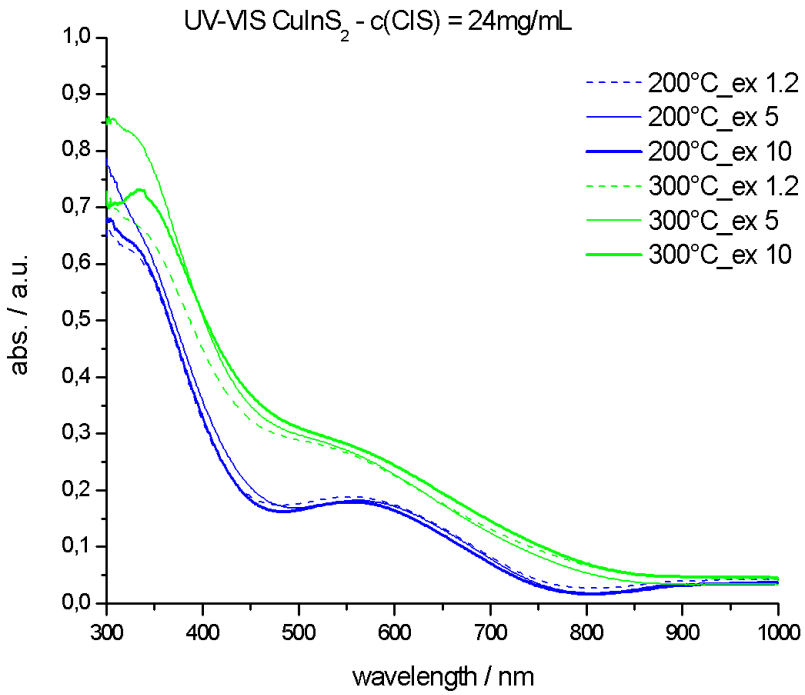

Figure 23: UV-Vis spectra of the $CuInS_2$ layers with differing amount of sulphur and annealing temperatures

In Figure 23 the UV-Vis spectra of the different samples at 200°C and 300°C are pictured. The samples that were annealed at 400°C were left out this interpretation because the layers of them were to thin to obtain valid results. A difference in layer thickness can sometimes occur as the samples were not fabricated all together but in groups of three due to the fact that the annealing step should take place immediately after the application of the $CuInS_2$ layer and only one tube furnace was available.

At the spectrum we can see, that the onset of the absorption peak, which has its maximum around 580 nm, is at 850 nm for the 300°C sample and the onset of the 200°C sample is at about 800 nm. This shift might be due to the fact that the crystallite size of the $CuInS_2$ nanocrystals is increasing with temperature, which was found out by the XRD measurements that are discussed in the following chapter. A smaller primary crystallite size increases the bandgap and therefore leads to a higher energy which is equal to lower wavelengths. Another reason for the blue shift of the 200°C sample might be interference occurrence as a result of differing layer thickness.

3.2.2 XRD Measurements

According to the Scherrer equation[75] (8) the average primary crystallite size of the $CuInS_2$-nanocrystals (d_{XRD}) was determined by the analysis of the x-ray diffraction measurements.

$$d_{XRD} \approx \frac{\lambda}{\Delta(2\theta) \cdot \cos\theta} \quad \textbf{(8)}$$

Δ(2θ) is the full width at half maximum (FWHM) of the peak in radians and θ is half of the scattering angle 2θ. Although it is a very good one, the Scherrer relationship is only an approximation for spherical crystals, not an equation having an overall and absolute validity. The nanocrystals size is inversely proportional to the FWHM.

The XRD measurements are pictured and the respective analyses of the primary crystallite size of the $CuInS_2$-nanocrystals are listed directly beneath. Figure 24, Figure 25 and Figure 26 show that at 200°C still a lot of impurities are present within the $CuInS_2$ layer but at 300°C the purity level is already very high and there are no side products existing anymore.

In Table 2, Table 3 and Table 4 the peaks that were used to do the calculations are listed together with the resulting data. The mean of the three peaks of each sample is calculated and these values are compared.

[75] Debye P., Scherrer P., *Physikalische Zeitschrift* **1916**, 17, 277-283

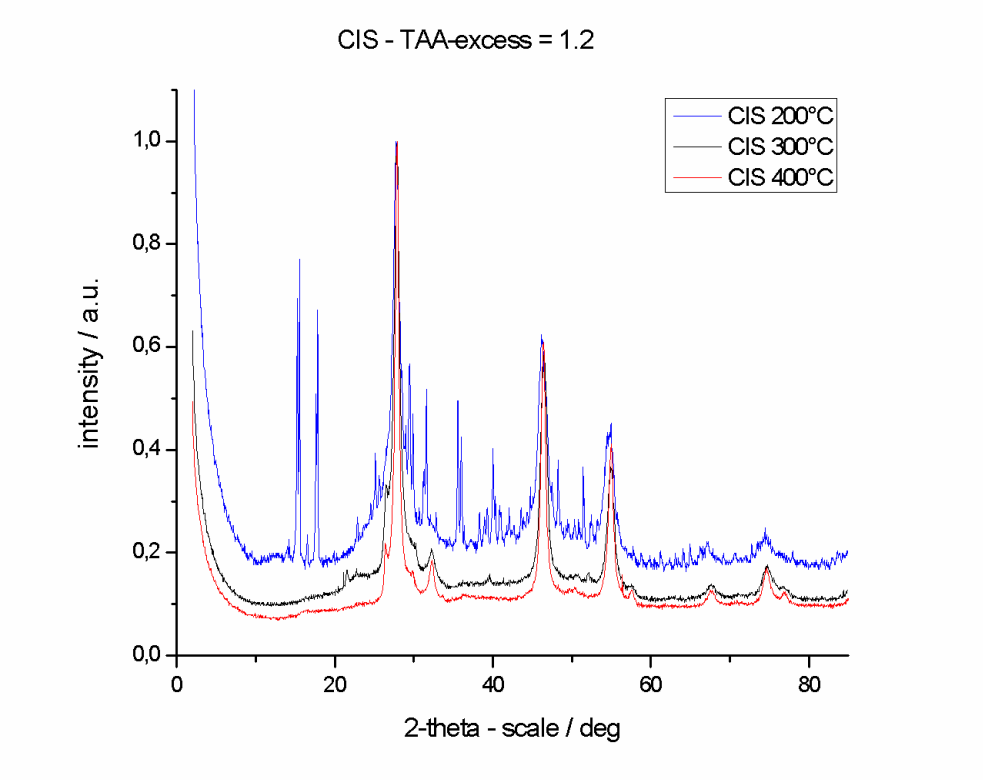

Figure 24: XRD measurements of $CuInS_2$ with a sulphur source excess of 1.2

Table 2: Data of the Scherrer analysis of the primary crystallite size of the $CuInS_2$-nanocrystals using a TAA-excess of 1.2

	2θ / deg	d / nm	average d / nm
CIS_01_200	27,762	8,31	
1.2 eq. TAA	46,185	7,64	
200°C	54,975	7,49	**7,81**
CIS_01_300	27,897	10,57	
1.2 eq. TAA	46,481	10,38	
300°C	54,923	10,22	**10,39**
CIS_01_400	27,902	16,79	
1.2 eq. TAA	46,435	15,28	
400°C	54,969	13,95	**15,34**

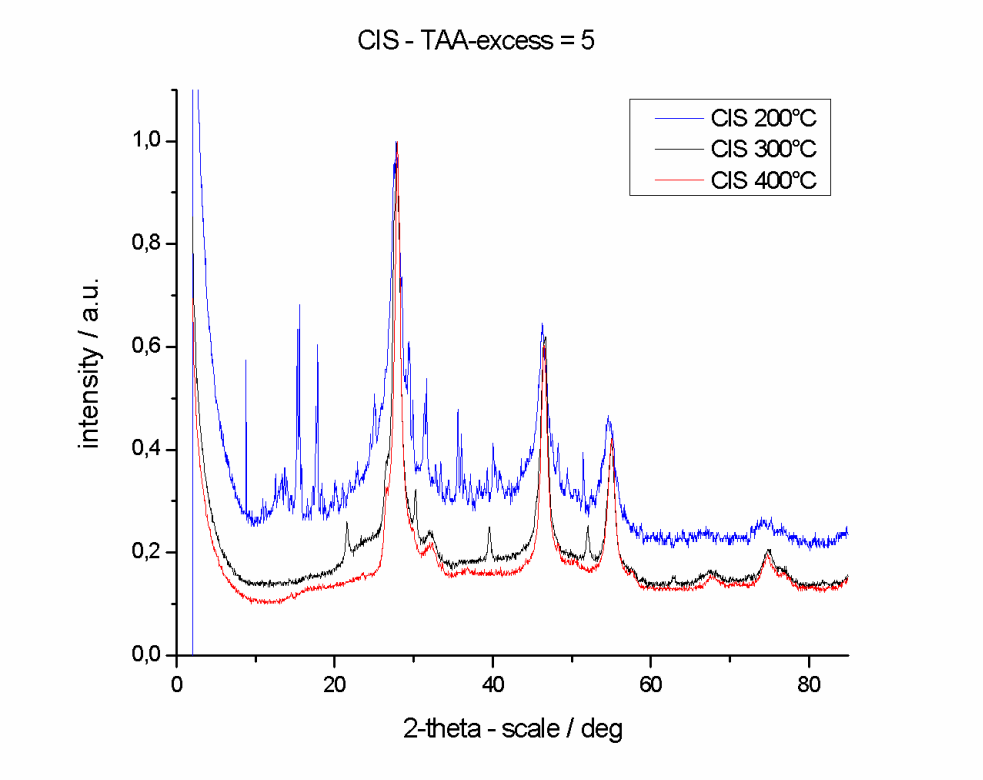

Figure 25: XRD measurements of $CuInS_2$ with a sulphur source excess of 5

Table 3: Data of the Scherrer analysis of the primary crystallite size of the $CuInS_2$-nanocrystals using a TAA-excess of 5

	2θ / deg	**d / nm**	**average d / nm**
CIS_02_200	27,761	9,17	
5 eq. TAA	46,185	7,92	
200°C	54,975	7,54	**8,21**
CIS_02_300	27,897	11,05	
5 eq. TAA	46,473	10,43	
300°C	54,923	10,35	**10,61**
CIS_02_400	27,902	16,95	
5 eq. TAA	46,432	15,09	
400°C	54,968	14,18	**15,41**

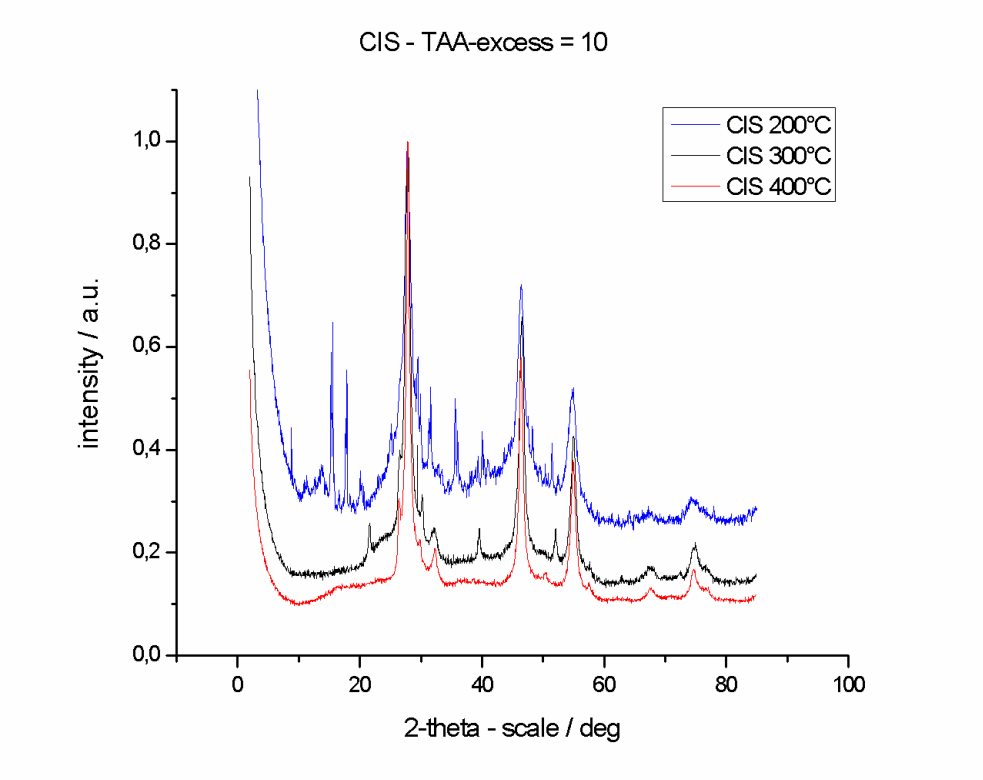

Figure 26: XRD measurements of $CuInS_2$ with a sulphur source excess of 10

Table 4: Data of the Scherrer analysis of the primary crystallite size of the $CuInS_2$-nanocrystals using a TAA-excess of 10

	2θ / deg	**d / nm**	**average d / nm**
CIS_03_200	27,824	7,01	
10 eq. TAA	46,53	7,75	
200°C	54,802	8,51	**7,76**
CIS_03_300	27,855	8,79	
10 eq. TAA	46,563	10,42	
300°C	55,001	10,07	**9,76**
CIS_03_400	27,855	13,92	
10 eq. TAA	46,403	14,43	
400°C	54,903	11,29	**13,21**

The Scherrer analysis evidenced that the primary crystallite size depends on the annealing temperature. At lower temperature the crystals are smaller than they are after a high temperature annealing step. The Scherrer method was applied for the three main peaks of every sample, leading to an average primary crystallite size of ~8

nm at 200°C, about 10.5 nm at 300°C and roughly 15 nm at 400°C. The values of the samples that were prepared out of the $CuInS_2$ solution with a TAA-excess of 10 are a bit lower than the others. Nevertheless it can be assumed that the TAA amount is not having a significant influence on the primary crystallite size, which definitely is controlled by the annealing temperature.

3.2.3 SEM Images

The idea of the inverse assembly bases on a nanostructured inorganic layer that shows porosity that enables the polymer the diffuse into the resulting holes forming together a photoactive layer with a large interface and without dead ends. Therefore the porosity and especially the pore size is an important characteristic of the inorganic layer and would be good to be controllable. The influence of the temperature and the degree of sulphur source excess was investigated by scanning electron microscopy and profilometer measurements (chapter 3.2.4) were done to proof the results.

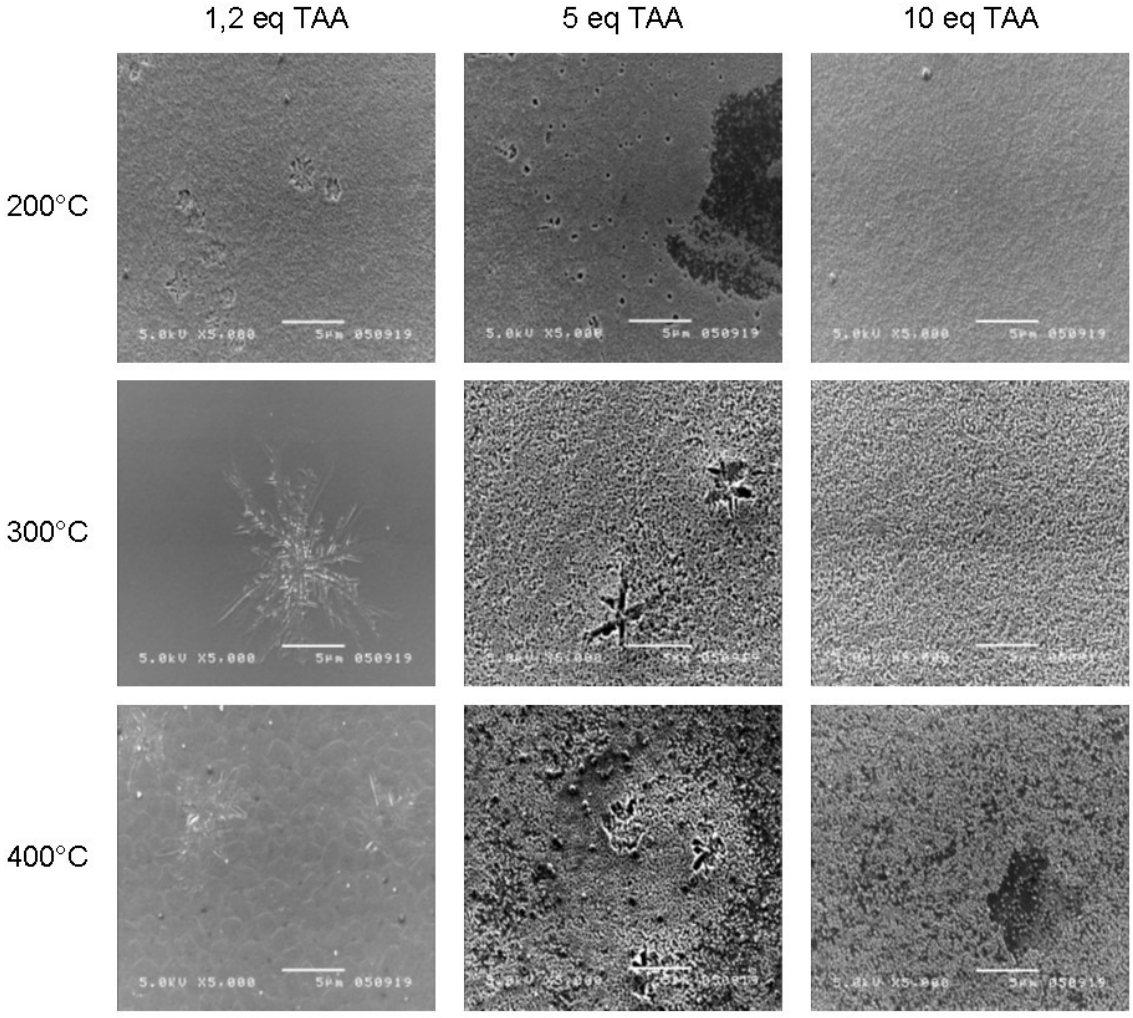

Figure 27: SEM pictures (5000x magnification) of the $CuInS_2$ layers prepared with differing TAA amount and differing annealing temperature.

In Figure 27 a matrix is pictured that shows SEM images of the $CuInS_2$ layers prepared out of solutions with differing TAA-excess and at different annealing temperatures. Although linear characteristics cannot be identified, it can be seen that with a TAA-excess of only 1.2 the layers do not show porosity at all especially at 300°C and 400°C and thus would not lead to the desired morphology in inverse solar cells. The surface morphology is considerably improved at the layers prepared with a 5-fold and 10-fold TAA-excess and is of higher porosity at higher temperatures as well. The highest pore size might be obtained using a 5-fold TAA-excess and an annealing temperature of 400°C, while the samples with 5-fold excess / 300°C and 10-fold excess / 400°C also show good surface morphologies for an application within inverse assembled nanocomposite solar cells.

3.2.4 Profilometer Measurements

The profilometer measurements give not only information about the average thickness of the layers but also about the roughness of their surface. This in combination with the SEM images leads to good conclusions about the layer surface constitution and its porosity. As the $CuInS_2$ layers prepared of out of a solution with a 5-fold TAA-excess turned out to be have the most porous surface, the profilometer measurement results of these layers at 200°C, 300°C and 400°C are pictured in Figure 28, Figure 29 and Figure 30. Figure 31 and show the profilometer measurements of the 1.2-fold excess / 400°C and the 10-fold excess / 400°C samples.

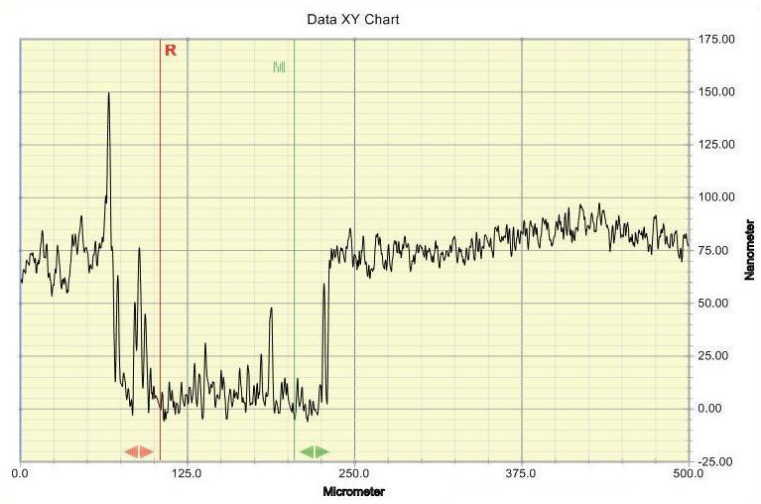

Figure 28: Profilometer measurements of $CuInS_2$ with a TAA-excess of 5 at 200°C

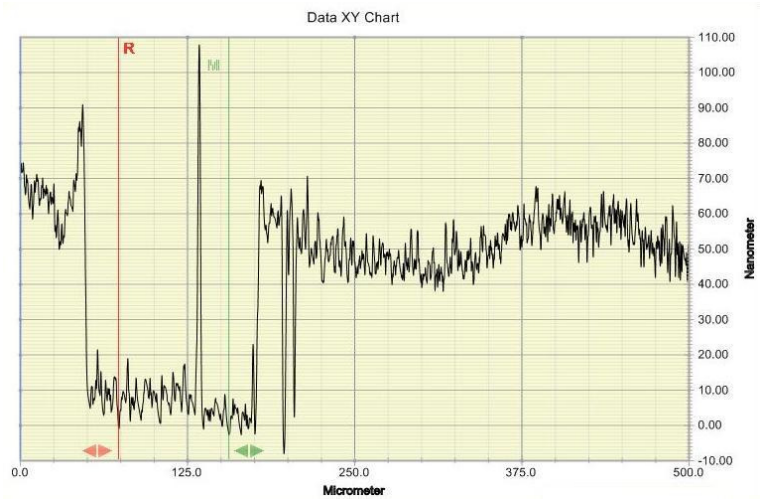

Figure 29: Profilometer measurements of $CuInS_2$ with a TAA-excess of 5 at 300°C

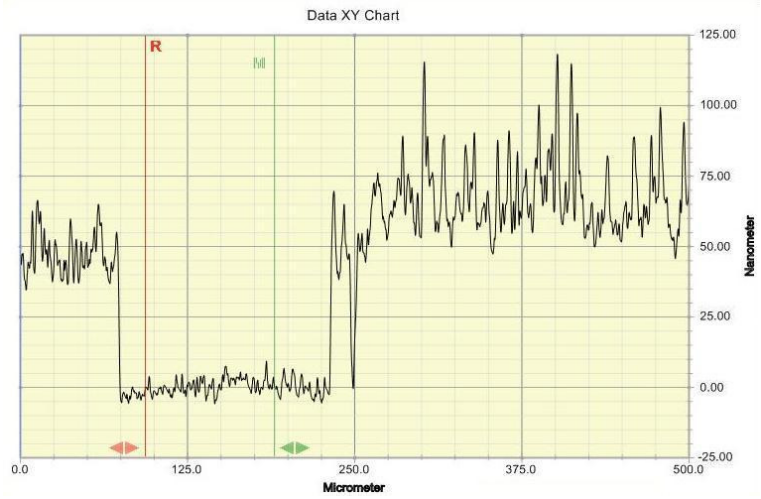

Figure 30: Profilometer measurements of $CuInS_2$ with a TAA-excess of 5 at 400°C

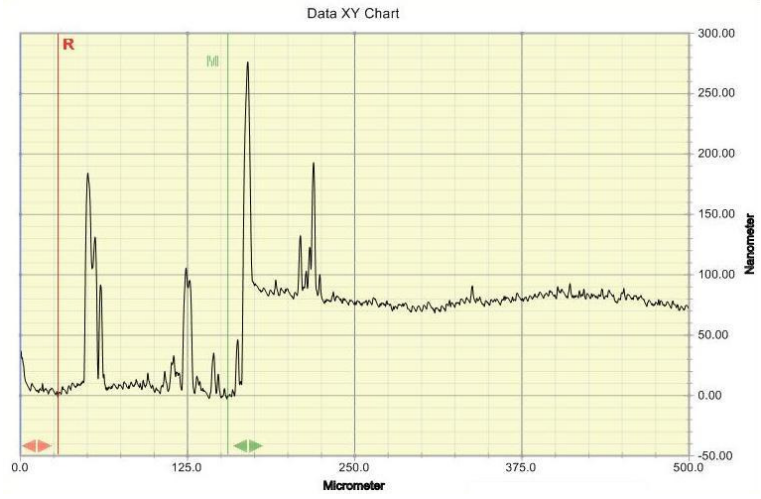

Figure 31: Profilometer measurements of $CuInS_2$ with a TAA-excess of 1.2 at 400°C

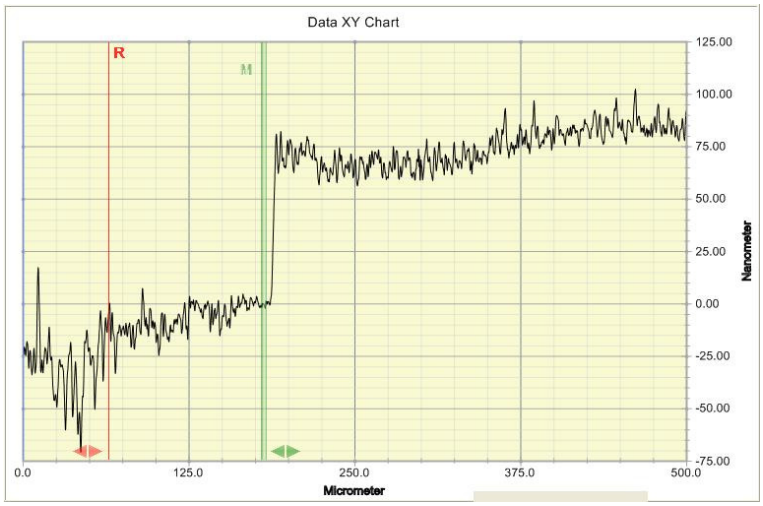

Figure 32: Profilometer measurements of $CuInS_2$ with a TAA-excess of 10 at 400°C

The profilometer measurements confirm the results of the SEM images as the layer surface show an increasing roughness with increasing annealing temperature. The results of the profilometer measurements are listed in Table 5 and Table 6.

Table 5: Results of the profilometer measurements of the $CuInS_2$ layers prepared out of a 5-fold TAA-excess solution

	5-fold exc. / 200°C	5-fold exc. / 300°C	5-fold exc. / 400°C
d_{layer} / nm	51.6	79.7	67.6
σ / nm	6.3	10.8	24.9

Table 6: Results of the profilometer measurements of the $CuInS_2$ layers annealed at 400°C

	1.2-fold exc. / 400°C	5-fold exc. / 400°C	10-fold exc. / 400°C
d_{layer} / nm	78.6	67.6	76.6
σ / nm	4.4	24.9	14.4

The standard deviation (σ) of the layer thickness, which displays a mean value, gives information about the roughness of the layer surface. Logically a higher standard deviation amplifies a rougher and so a larger $CuInS_2$ layer surface. The results show that an enormous increase of the roughness of the $CuInS_2$ surface takes place at an

annealing temperature of 400°C. As estimated, the surface of the 1.2-fold excess / 400°C sample has a very plane surface, which underlines the results of the SEM imaging that indicate the 1.2-fold excess layer as inappropriate for nanocomposite solar cell applications. After the SEM imaging we would have expected the 5-fold excess / 300°C sample and the 10-fold excess / 400°C sample to show a little higher degree of roughness, but in fact all data obtained by these measurements are consistent with the trend of the SEM images. Higher annealing temperatures lead to a higher degree of layer roughness and so to a larger surface, which is desirable for nanocomposite solar cells. The $CuInS_2$ layers, which were prepared out of a solution with a 5-fold TAA-excess, show the highest porosity and hence they are the most interesting for solar cell preparation.

3.2.5 AFM Measurements

Atomic force microscopy was also done on a 5-fold excess / 400°C sample. Figure 33 shows two pictures of this layer which proof the results of the other investigations. On the left we can see an overview of the layer and on the right the layer is depicted at a higher magnification, which shows very clearly the holes. From the left picture we can also get an idea of the form of the holes. They have different forms as there are round holes as well as very long and deep ones. This sample was bit thicker, having an average thickness of 98 nm, which neither better nor worse than the bit lower thicknesses that were obtained at the profilometer measurements.

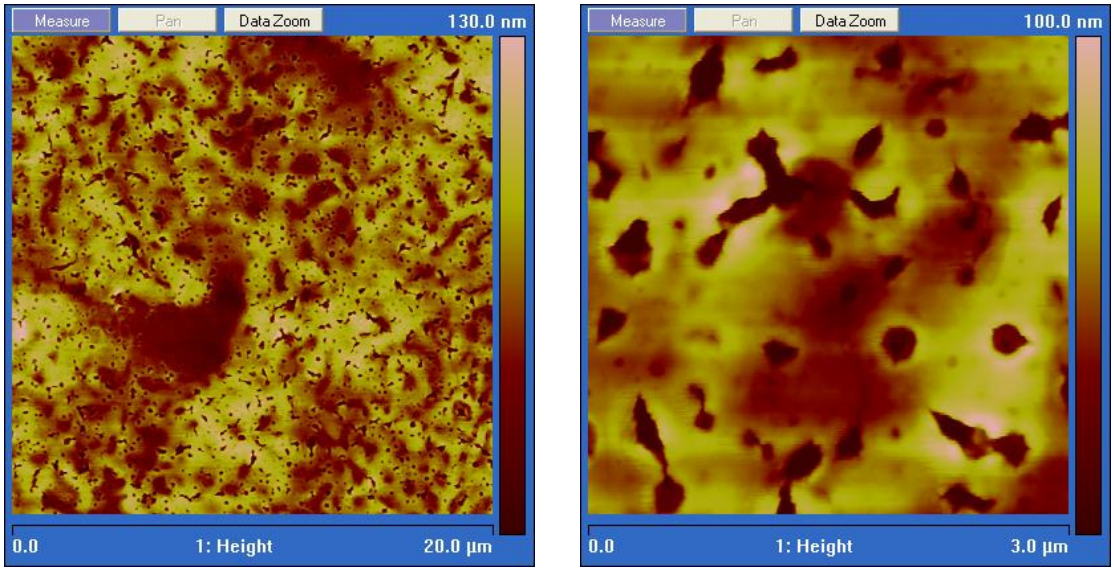

Figure 33: AFM images of the $CuInS_2$ layer that was spin coated out of a solution with a 5-fold TAA excess and annealed at 400°C at two different magnifications.

3.3 Inverse Nanocomposite Solar Cells

The investigations on the $CuInS_2$ layers showed that they are applicable as acceptor material in nanocomposite solar cells. Therefore, in the next step, the layer formation on ITO covered glass substrates was investigated in order to obtain inverse nanocomposite solar cells. The preparation of the inverse solar cells turned out to be much more difficult than expected due to wetting problems. Figure 34 shows some pictures of the $CuInS_2$ layers spin coated onto the ITO film after the annealing step, which recorded with the light microscope. A lot of work was done to improve the wetting abilities of the $CuInS_2$ layer on ITO. However, in any case, full coverage of the ITO surface (which has a blue colour in the images) was never obtained. Also, other coating solutions, including a small amount of Zn salt (4.5.2) were investigated as well as different spin parameters were tested. Furthermore it was tried to improve the wettability of the ITO film through changed pre-treatment processes. ….. was add to the ultrasonic water bath, within another type series the ultrasonic water bath was left out at all and at another time the devices were cleaned with acetone a second time immediately before the $CuInS_2$ layer was applied by spin coating. None of the experiments led to significant improvement, therefore it was not possible to prepare inverse nanocomposite solar cells yet.

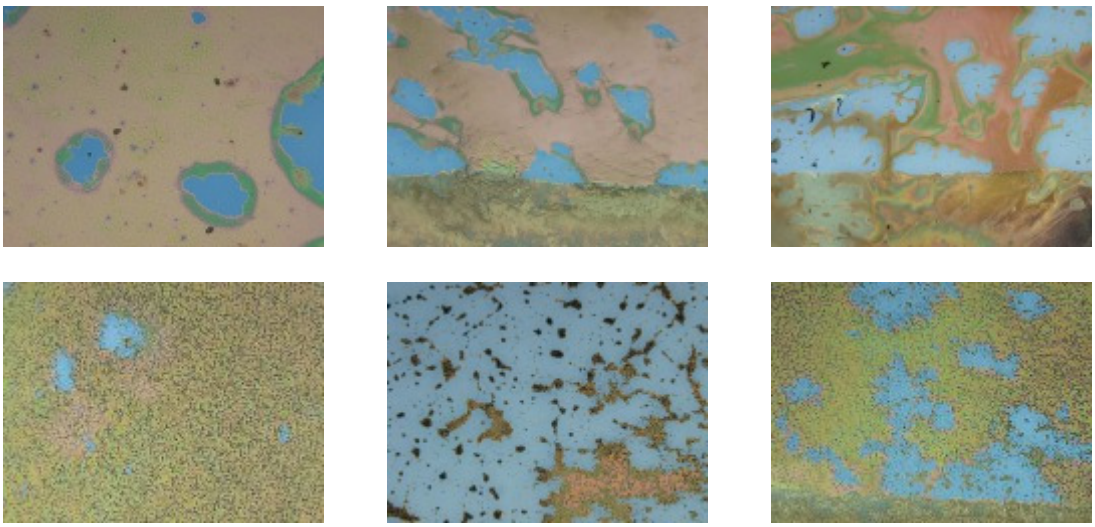

Figure 34: Pictures of $CuInS_2$ layers after the annealing step that proof their poor wetting behaviour on ITO.

However, it was possible to obtain a bilayer heterojunction solar cells with the common assembly that was glass / ITO / P3EBT / $CuInS_2$ / Al were prepared as described in chapter 4.4.3. For the thermal heating step, a temperature of only 180 °C was used,

which is not the optimum temperature for the $CuInS_2$ formation but was necessary due to the low thermal stability of the polymer. Surprisingly, these nanocomposite bilayer solar cells already reached a efficiency of 0.24 %. Surprisingly because we have to consider that the bilayer assembly is strongly disadvantaged due its small donor-acceptor interface that is leading to a poor exciton diffusion yield, which is discussed in detail in chapter 2.1 as well as that the inorganic sulphide formation is not fully completed.

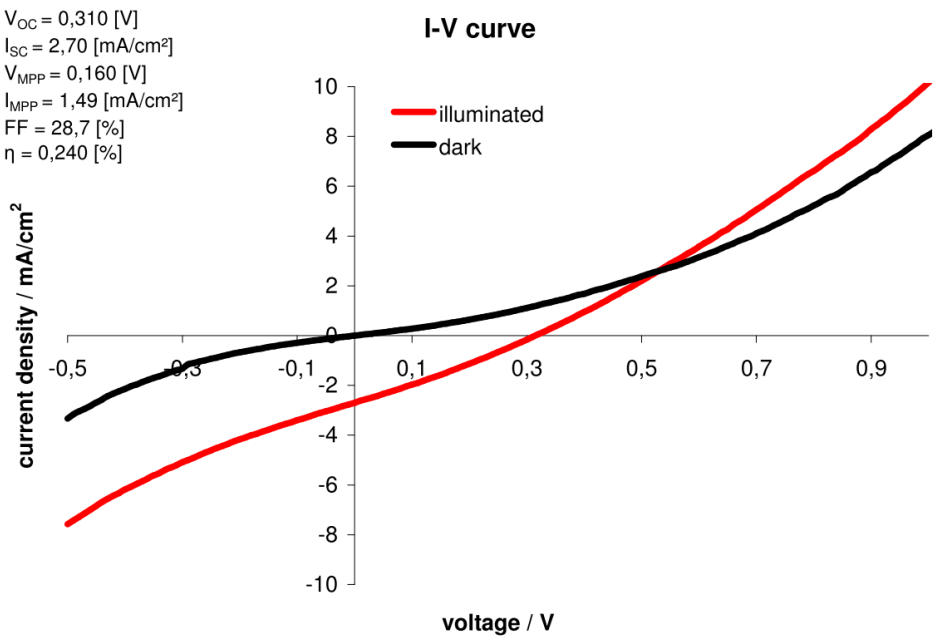

Figure 35: I-V curve of a P3EBT/$CuInS_2$ bilayer heterojunction solar cell

Figure 35 shows the I-V characteristics of the best performing solar cell of a type series that included many solar cells with efficiencies within the range of 0.1 to 0.2 %.

Nevertheless the idea of the inverse nanocomposite solar cell should be the further investigated, as the preliminary tests on the $CuInS_2$ layers were very promising concerning the controllability of their surface morphology as well as the reached efficiencies for the disadvantaged bilayer assembly were. One possible solution could be the use of different solvent or solvent mixtures or of surfactants in the coating solution.

4 Experimental Work

4.1 Used Chemicals and Materials

All solvents, chemicals and materials that were used for the preparation of inorganic layers, hybrid and nanocomposite solar cells are listed in Table 7.

Table 7: List of chemicals and materials used for the experimental work

chemicals / materials	**purity / properties**	**source of supply**
2 – propanole	puriss.	Sigma Aldrich
Acetone	puriss.	Sigma Aldrich
Aluminium	wire, 1.0mm diam., 99.98%	Umicore
Chloroform	CHROMASOLV, ≥ 99.999%	Sigma Aldrich
Chloroform	puriss. p.a.	Sigma Aldrich
Copper (I) iodide	purum, ≥ 99,0%	Riedel-de Haën
Copper (I) acetate	99,999%	Aldrich
Gold	wire, 1.0mm diam., 99.99%	Aldrich
Hydrochlorid Acid	37% - 38%, fuming	J. T. Baker
Indium (III) chloride	98%	Aldrich
Indium (III) chloride	99,999%	Aldrich
ITO-covered glass substrates	15 x 15 mm, R_S 15 – 25 Ω	Delta technologies
P3EBT	90% - 93% regioregularity	Rieke Metals, Inc.
P3HT	ADS306PT, regioregular,	American Dye Source

PCBM [C60]	99,5%	Solenne
PEDOT:PSS	Baytron P VPAI4083	HC. Starck
PEDOT:PSS	Baytron P Form .CPP 105D	HC. Starck
Pyridine	CHROMASOLV, ≥ 99.9%	Sigma Aldrich
Thioacetamide	puriss. p.a., ≥ 99,0%	Fluka
Thiourea	puriss. p.a., ≥ 99,0%	Fluka
Titanium	wire, 1.0mm diam., 99.99%	Aldrich
Zinc acetate	99,99%	Aldrich
Zinc chloride	purum, ≥ 98,0%	Fluka
Zinc powder	< 10 µm, ≥ 98%	Aldrich

Further details on the used chemicals are listed in chapter 6.2.

4.2 Pre-treatment of the Substrates

To optimize the terms of condition for the applying of the different organic and inorganic layers as well as their usability for fabricating solar cells, the ITO-covered glass substrates have to be pre-treated accurately. The process of pre-treatment consists of two main parts, the chemical etching of the substrates followed by the cleaning process. Both are described more in detail in the following chapters.

4.2.1 Chemical Etching

This step has to be done due to the low thickness of the photoactive layer and the used way of measuring the I-V characteristics of the solar cells. As already mentioned the thickness of a completed solar cell, varies from 400 to 800 nm including the electrodes. The photoactive layer, reaches a maximum thickness of roughly 200 (organic solar cells) – 400 (nanocomposite solar cells) nm.

The first step of analysing a solar cell is always the measurement of the I-V characteristics. In this case the solar cells were channelled into a Glove Box, where the electrodes of the solar cell were contacted with test prods. A measurement tip can easily transfix the upper electrode and the photoactive layer so that it is not only in contact with the upper electrode, but also with the lower one. In that case you create a short circuit and get wrong measurement data for the I-V characteristics.

To avoid that case, a part of the ITO layer on the glass substrate was removed by chemical etching. Therefore some adhesive tape was put on the major area of the ITO coated side of the device and dipped the whole substrate with some zinc powder into fuming hydrochloride acid 37% p.a., two times in a row so that the ITO was cleared away from the not covered part of the substrate. The rest of the hydrochloride acid was washed with water and afterwards the adhesive tape was removed.

4.2.2 Cleaning of the Substrate

The cleaning process started with acetone at the beginning, followed by two ultrasonic baths at 50 °C. At first the substrates were put into a water bath for 20 – 30 minutes and afterwards into a bath of isopropanol for the same time. Ideally a solar cell was built within one working day; otherwise the substrates were pre-treated on one day and

stored in the isopropanol bath over night (room temperature) in order to start with the preparation next morning.

After every treatment with a solvent (acetone, water, isopropanol) the substrates were cleaned with a non-fuzzing tissue and the dust was removed by a stream of carbondioxide gas, but especially after the last ultrasonic bath this part of the cleaning process was done very carefully.

4.3 General Preparation Techniques and Procedures

During this work several solar cells consisting of various films with different kinds of compounds have been prepared. The different types of fabricated solar cells are listed in Table 8.

Table 8: Different types of prepared solar cells

Type of Solar Cell	Type of Assembly	Photoactive Layer	
		donor	acceptor
polymer/fullerene solar cell	bulk-heterojunction	P3HT	PCBM
polymer/fullerene solar cell	inverted bulk-heterojunction	P3HT	PCBM
nanocomposite solar cell	Bilayer	P3EBT	CIS
nanocomposite solar cell	inverted bilayer	P3EBT	CIS

For all of the different solar cells, the steps of preparation are nearly the same:

- layer application by spin coating
- annealing step
- evaporation of metal electrodes.

These steps of the preparation of organic solar cells are described detailed in the following chapters 4.3.1, 4.3.2 and 4.3.3. If not described in another way all the experiments were performed with the equipment mentioned below

4.3.1 Spin Coating

A CT62 spin coater produced by the company Karl Suss Technique was used to do the spin coating of the different solutions. That equipment offers the separated adjustment

of speed and acceleration of the turntable and in addition the possibility to run two cycles of different speed and acceleration in a row.

4.3.2 Annealing Step

In general an assembling of Heidolph instruments consisting of a MR Hei-Standard magnetic stirrer combined with an EKT Hei-Con external control unit and a temperature sensor was used for the experiments on polymer/fullerene solar cells.

The thermal treatment of the nanocomposite solar cells generally has been taken place in a tube furnace from Nabertherm (R50/500/12 in combination with a controller P330). In some cases a tube furnace from Heraeus (RO 4/25 in combination with a controller RE 1.1) was used.

4.3.3 Evaporation of Metal Electrodes

The metal electrodes were applied by evaporation, which started at a vacuum higher than 2.10^{-5} mbar. Either the evaporation unit MED 010 or MED 020 from Baltec was used. In order to get structured electrodes of a well defined area the devices were covered with shadow masks. The evaporation in the MED 020 was carried out bottom-up using two tungsten boats, while the MED 010 only has one tungsten coil using the top down evaporation method. Therefore the MED 020 was very useful to apply the Titan – Aluminium – Titan electrode on the glass devices to fabricate the inverted type of bulk-heterojunction solar cells. In addition the MED 020 was also equipped with an oscillating quartz crystal to measure the layer thickness during the evaporation

4.4 Preperation of Solar Cells

4.4.1 Front Side Assembled P3HT/PCBM Bulk Heterojunction Solar Cells

The PEDOT:PSS solution (Baytron P VPAI 4083) was spin coated on the etched and cleaned substrates with a speed of 2500 rpm for 30 seconds at an acceleration of 200 rpm/s. - 2500 / 200 / 30 in short (this kind of notation is used in the following).

A solution of 30.0 mg (0,033 mmol, 1 eq) PCBM and 25.0 mg (0,12 mmol, 3.6 eq) P3HT in 3 ml Chloroform CHROMASOLV 99.999% was prepared in a glass vial by

stirring for 1 hour and heating up to 50 °C for 15 minutes in inert atmosphere. Meanwhile the PEDOT:PSS layer was dried at 100°C for 10 minutes. Accordingly the solution of the photoactive P3HT/PCBM-layer was applied by spin coating with the following parameters: 1000 / 1000 / 60.

After the evaporation of the Aluminium electrode, another heating step had taken place. The completed solar cells were heated to 150°C for 10 minutes in inert atmosphere by the heating plate. The design of this solar cells was: glass / ITO / PEDOT:PSS / (P3HT/PCBM) / Al. Figure 36 shows a flow diagram of the preparation steps.

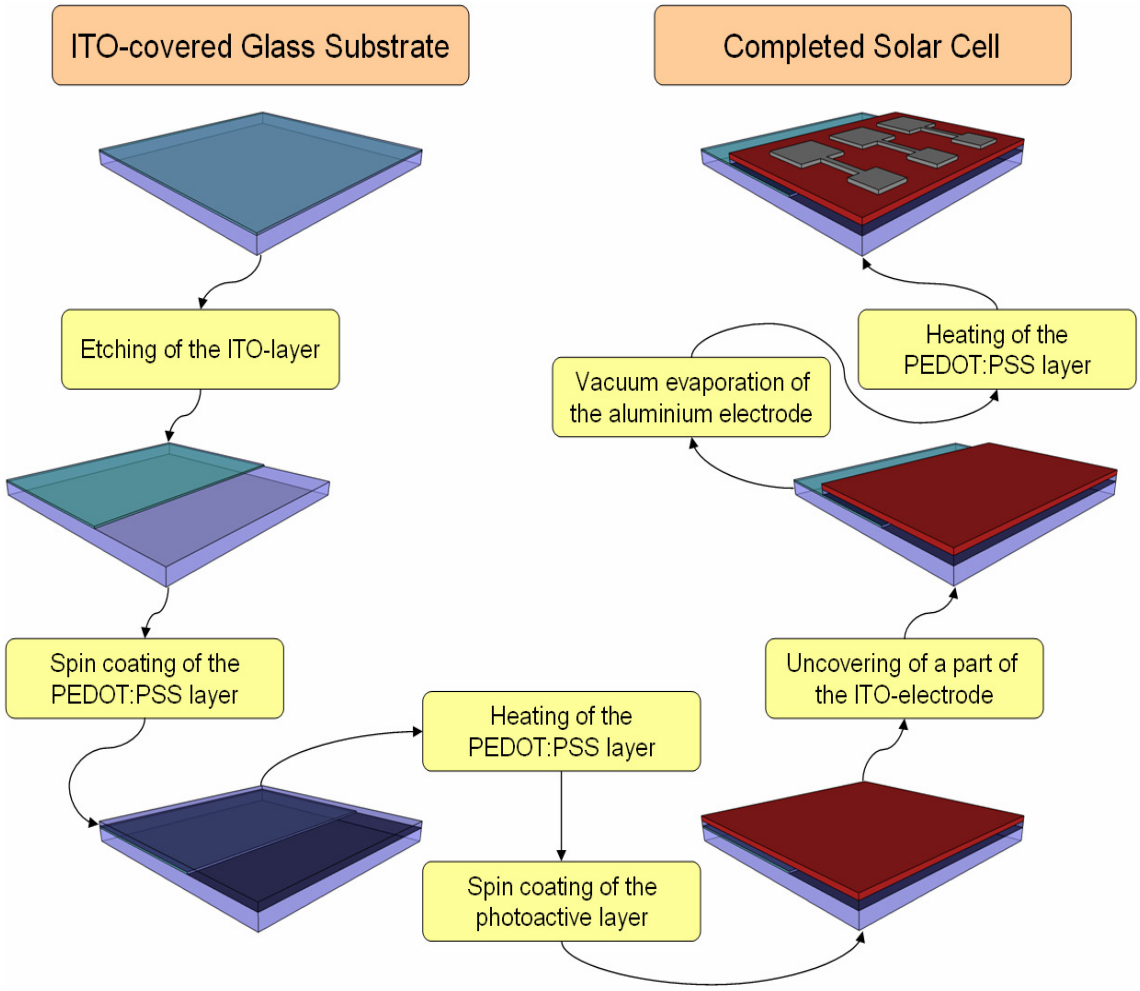

Figure 36: Flow diagram of the preparation steps of a P3HT/PCBM bulk heterojunction solar cell

4.4.2 Back Side Assembled P3HT/PCBM Bulk Heterojunction Solar Cells

The assembling of these solar cells was: glass / Ti / Al / Ti / (P3HT/PCBM) / PEDOT:PSS / Au. Aluminium was evaporated onto the full area of the cleaned glass substrates by leaving out a stripe of approximately 4 mm, due to the same reason as the etching of the ITO layer is done by the normal designed solar cells – to avoid short circuits.

After that the P3HT/PCBM layer was spin coated with 1000 rpm for 60 seconds at an acceleration of 1000 rpm/s. The synthesis of the solution was done the same way as described in chapter 4.4.1. By skipping an annealing step at this stage the cells were just leaved at room temperature for some minutes before applying the PEDOT:PSS solution (Baytron P Form .CPP 105D), which was spin coated at 2500 / 200 / 30.

As electrode, gold was evaporated, before the final annealing step had taken place at 150 °C for 10 minutes in inert atmosphere on the heating plate.

4.4.3 P3EBT/CIS Bilayer Solar Cells

The construction of these solar cells was: glass / ITO / P3EBT / CIS / Al. A solution of the polymer (6 mg/ml) was spin coated onto the etched and cleaned substrates with the following settings: 2000 / 2000 / 20. The P3EBT – layer was annealed at 120 °C for 10 minutes under inert conditions on a heating plate. After that the $CuInS_2$ solution was synthesized the way described in chapter 4.5.1 and spin coated by the same settings as the polymer was. Another annealing step was carried out at the tube furnace of Heraeus. The sample was heated to 80 °C within 3 minutes before being heated to 180 °C within 20 minutes. In the following heating rates in the tube furnace will be described like this: 3min ↑80°C / 20min ↑180°C / 14min ↔180°C. At this temperature the sample was kept for 14 minutes. The last step was to deposit the aluminium electrodes by evaporation.

4.4.4 P3EBT/CIS Inverted Bilayer Solar Cells

The design of these solar cells was: glass / ITO / CIS / P3EBT / Al. The $CuInS_2$ solution was synthesized as described in chapter 4.5.1 and spin coated onto the etched and cleaned substrates with the parameters 2000 / 2000 / 20. The samples have been

annealed in the tube furnace of Heraeus by using the following heating rate: 3min ↑80°C / 20min ↑180°C / 14min ↔180°C.

A P3EBT solution of 6 mg/ml was spin coated with the common used settings of 2000 / 2000 / 20 and annealed on a heating plate at 120 °C for 10 minutes in inert atmosphere. The aluminium electrodes were evaporated by using the MED 020 as always.

4.5 Fabrication of $CuInS_2$ Thin Films

4.5.1 $CuInS_2$

A mixture of 76.2 mg CuI (0.4 mmol, 1 eq.), 176.3 mg $InCl_3$ (0.8 mmol, 2 eq.) and 150.3 mg TAA (2.0 mmol, 5 eq.) was dissolved in 4 ml Acetonitril. The mixture was stirred on a magnetic stirrer at room temperature for one hour.

4.5.2 $CuInS_2$ / Zn

A mixture of 5.4 mg $ZnCl_2$ (0.04 mmol, 0.1 eq.), 76.2 mg CuI (0.4 mmol, 1 eq.), 176.3 mg $InCl_3$ (0.8 mmol, 2 eq.) and 150.3 mg TAA (2.0 mmol, 5 eq.) was dissolved in 4 ml Acetonitril. The mixture was stirred on a magnetic stirrer at room temperature for one hour.

4.5.3 $CuInS_2$ - XRD Test Series

For the preparation of $CuInS_2$ thin films the TAA-route without zinc was used. A concentration of 24 mg/ml $CuInS_2$ turned out to be the most practical one to do the X-ray diffraction measurements. Within this test series the influence of the annealing temperature and the sulphur excess in the solution, on the crystallinity in the $CuInS_2$ layer was investigated. Therefore not only the heating temperature but also the amount of thioacetamide in the solution was varied. The following solutions were prepared.

$CuInS_2$ - 10

To get a tenfold excess of sulphur within the $CuInS_2$ solution, 94.2 mg CuI (0.5 mmol, 1 eq.), 218.9 mg $InCl_3$ (1.0 mmol, 2 eq) and 743.6 mg TAA (9.9 mmol, 20 eq) were dissolved in 5 ml Acetonitril.

$CuInS_2$ - 5

94.2 mg CuI (0.5 mmol, 1 eq.), 218.9 mg $InCl_3$ (1.0 mmol, 2 eq) and 371.8 mg TAA (4.9 mmol, 10 eq) were dissolved in 5 ml acetonitril. The excess of sulphur amounts 5.

$CuInS_2$ - 1.2

94.2 mg CuI (0.5 mmol, 1 eq.), 218.9 mg $InCl_3$ (1.0 mmol, 2 eq) and 89.2 mg TAA (1.2 mmol, 2.4 eq) were dissolved in 5 ml Acetonitril. The excess of sulphur amounts 1.2.

Afterwards all the mixtures were stirred on a magnetic stirrer at room temperature for one hour. The solutions were clear and according to the amount of sulphur more yellow coloured.

A defined volume of 1 ml of each of the produced solutions was dropped on three glass plates dimensioned 25 x 50 mm. The drop coating was done on a heating plate at 50°C to accelerate the evaporation of the solvent. After 10 minutes one plate of each of the three solutions was heated up to 200°C, 300°C and 400°C in the tube furnace in vacuo conditions by using the following heating rates:

- 7min ↑200°C / 15min ↔200°C
- 7min ↑300°C / 15min ↔300°C
- 7min ↑400°C / 15min ↔400°C

The prepared films were scrapped off the glass plates and the received dark coloured powders were used for X-ray diffraction measurements.

4.6 Measuring Equipments and Characterisation Methods

4.6.1 I–V characteristics

I-V characteristics of the solar cells were measured in a glove box in N_2-atmosphere with a Keithley 2400 source meter. The I-V curves were recorded under illuminated and dark conditions. A halogen lamp (250W, 24V) was used for illumination through a borosilicate glass window at the bottom of the glove box. The lamp was fixed in a distance of 20 cm to the sample and the light reached the sample with an intensity of 100 mW/cm^2. The scan rate of the Keithley 2400 source meter was 10 s^{-1}. Analyses of the recorded I-V characteristics were done by a software program that was written by me to facilitate the analysing process. The analysis tool is described in chapter 6.1 in detail.

4.6.2 UV-Vis

A Shimadzu UV-1800 UV-Spectrophotometer in combination with the software UVProbe 2.31 was used for measuring UV-Vis spectra.

4.6.3 Scanning Electron Microscopy SEM

Scanning electron microscopic pictures (SEM) were made on a JEOL JSM-5410 Scanning Microscope. They were very helpful to get further information on the constitution and the nature of the surfaces of the inorganic films.

4.6.4 IPCE-Spectroscopy

To be able to record IPCE spectra in inert atmosphere a special measurement chamber was designed at our working group by Thomas Rath. The layout of this measuring cell is depicted in Figure 37. The window is made of quartz glass and the housing consists of stainless steel. The contact to the solar cells is provided by copper wires, which pass the chamber through a ceramic inset in the wholes at the wall of the chamber. Connection to the Keithley 2400 source meter is done by coaxial cables.

(a) (b)

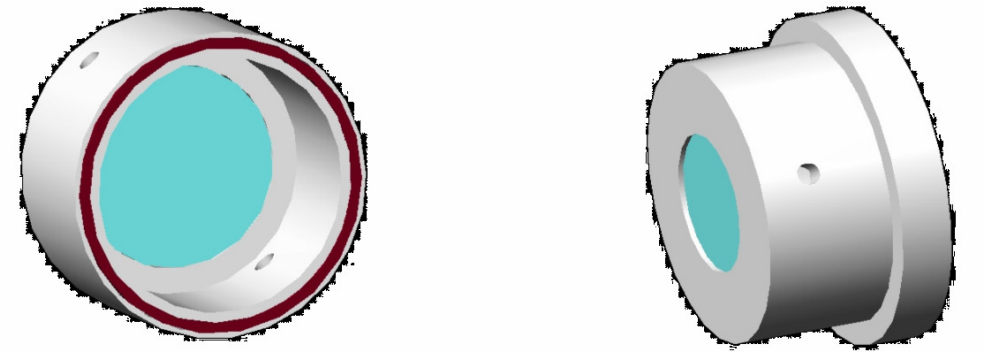

Figure 37: Sketch of the (a) open and (b) closed IPCE measuring cell to record spectra under inert atmosphere.[16]

Monochromatic light for the measurement was provided by the monochromator MuLTImode4 (wavelength range: 250 – 1100 nm) equipped with a 75 W Xenon lamp provided by AMKO. The silicon photodiode used for reference measurements was spectrally calibrated and fabricated by Hamamatsu (S 1226 series)[16].

4.6.5 X-ray Diffraction XRD

X-ray diffraction (XRD) patterns were detected to get further information on the crystallographic structure of the nanocrystals. Therefore a Siemens D 501 diffractometer in Bragg-Brentano-geometry operated at 40 kV and 30 mA, using Cu K_α radiation (λ = 1.54178 Å) at a scan rate of 0.05° (50 seconds measurement time per step) was used. By detecting the X-ray diffraction patterns it was able to determine the average primary crystallite sizes of the $CuInS_2$ layers (d_{XRD}) according to the broadening of the diffraction peaks using the Scherrer relationship(8).

For the calculation of the primary crystallite sizes of the $CuInS_2$-nanocrystals the main peaks of the XRD are used. These peaks and their data resulting from the Scherrer equation are listed in Table 2, Table 3 and Table 4. By measuring a Si-reference standard (NIST 640c), the experimental line width was determined to be 0.12° at the 2θ – position.

4.6.6 Profilometer

A Veeco Dektak 150+ Surface Profilometer was used to perform the measurements of the film thickness and roughness.

4.6.7 Light Microscopy

An Olympus BX60F5 light microscope in combination with an Olympus E520 digital camera was used to take the microscope pictures of the samples.

4.6.8 Atomic Force Microscopy AFM

AFM images were recorded on a Dimension Y Scanning Probe Microscope, equipped with a Hybrid XYZ scanner and a NanoScope V controller. EasyAFM was used as PC software package to handle the equipment.

5 Conclusion and Outlook

The topic of this thesis was the investigation of alternative assembly strategies for organic and nanocomposite solar cells. The active layer of these solar cells consists either of a mixture of two organic semiconductors or of a mixture of an inorganic with an organic one. In the first part, two different assembly strategies of organic solar cells have been investigated using as example the donor-acceptor system P3HT/PCBM. In the second part the preparation of porous $CuInS_2$ layers were researched to get information about their applicability as acceptor material in nanocomposites and especially inverse nanocomposite solar cells.

Within the first part of this work P3HT/PCBM bulk-heterojunction solar cells were prepared using the common assembly starting from the transparent ITO electrode and ending with aluminium as back side electrode. Efficiencies up to 3.7% were obtained, which are rather good values for this kind of solar cells especially considering that this result was achieved under atmospheric conditions and using chloroform as solvent. These solar cells showed an open circuit voltage of 660 mV, a short circuit current density of 11.3 mA/cm^2 and a fill factor of 49.7 %. The second assembly started from the back side electrode. Also aluminium was used, but to prevent the formation of an aluminium oxide layer, a thin layer of 3 nm Ti was applied on top of it. The transparent front side electrode consisted of a layer of PEDOT:PSS with a 5 nm gold layer on top. As we can see in Figure 38, where the I-V curves of both assembly types are compared, the back side assembled solar cell shows similar values for I_{SC} (11.5 ma/cm^2) and V_{OC} (600 mV) but a significantly poorer fill factor (31.4 %), which leads to less performance (η=2.18 %).

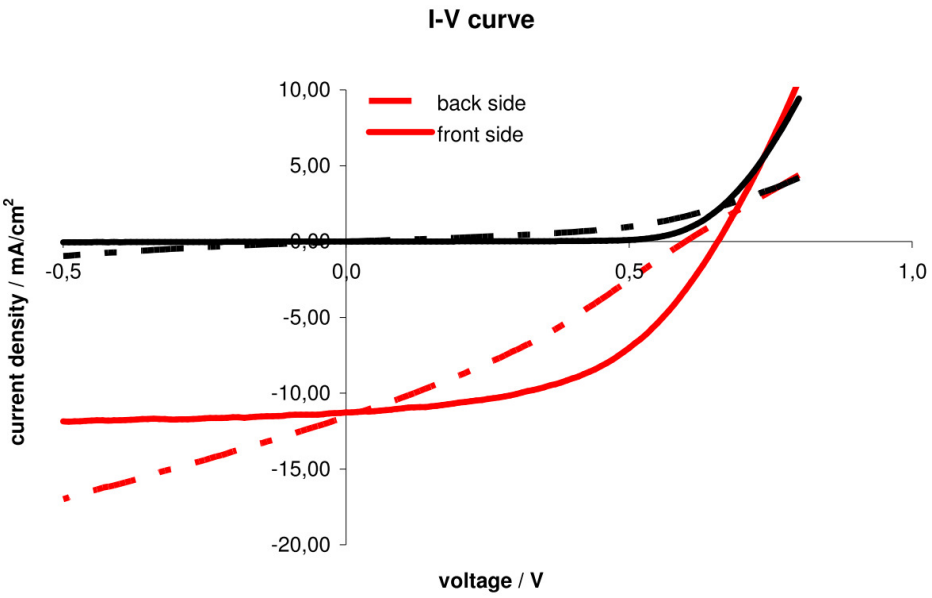

Figure 38: Comparison of the I-V characteristics of the front side and the back side assembled P3HT/PCBM solar cells

These results were reproducible as the reached efficiencies within the last type series' show in Figure 39.

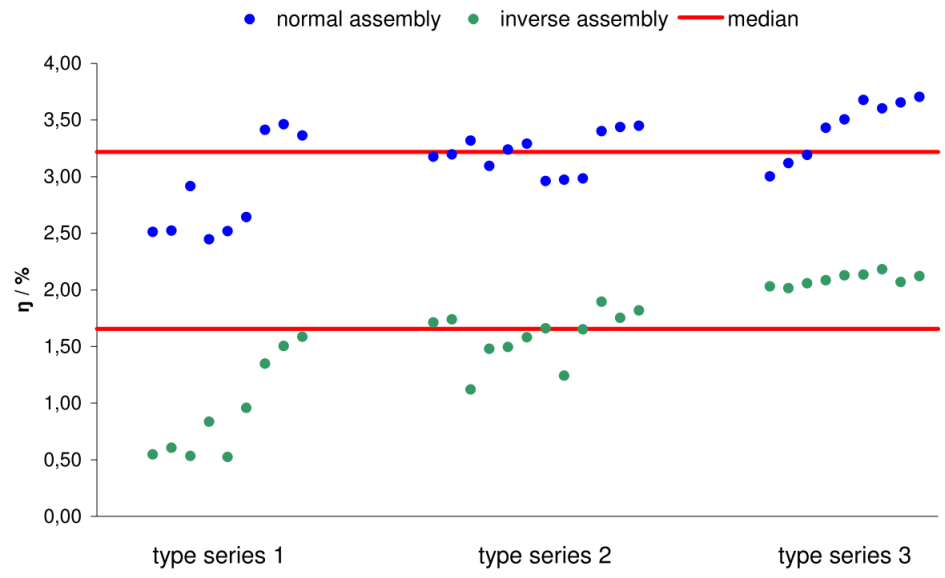

Figure 39: Achieved efficiencies within the last three type series' of front side (blue) and back side (green) solar cells. The median is marked in both cases by a red line.

The poorer fill factor of the back side assembly as well as the lower I_{SC} could be a consequence of non optimum layer thickness. Whereas for the front side assembled solar cells a layer thickness of 180 nm was found, which is in the optimum range reported for the P3T/PCBM system[73] the back side assembled solar cell exhibit a thicker active layer.

Although that means that absorption may be better, probably the charge transport is hindered because of the low mobility in the polymer phase. However, this approach is very promising as it omits the expensive ITO layer. For further optimisation, the layer thickness of the P3HT/PCBM nanocomposite mixture has to be tuned.

In the second part, the formation of porous $CuInS_2$ layers for application as acceptor material in nanocomposite solar cells has been investigated. By varying the concentration in the starting $CuInS_2$ precursor solutions and by using different annealing temperatures the morphology could be tuned and porous surfaces have been obtained which are very interesting for the preparation of inverse nanocomposite solar cells. At low temperatures (200 °C) impurities are still present but using higher temperatures an almost pure $CuInS_2$ layer has been obtained (Figure 40). The porosity of the layers depends on the amount of thioacetamide as well as on the used temperature. High temperatures and high amounts of thioacetamide are advantageous for a high porosity that is probably caused by the decomposition of thioacetamide.

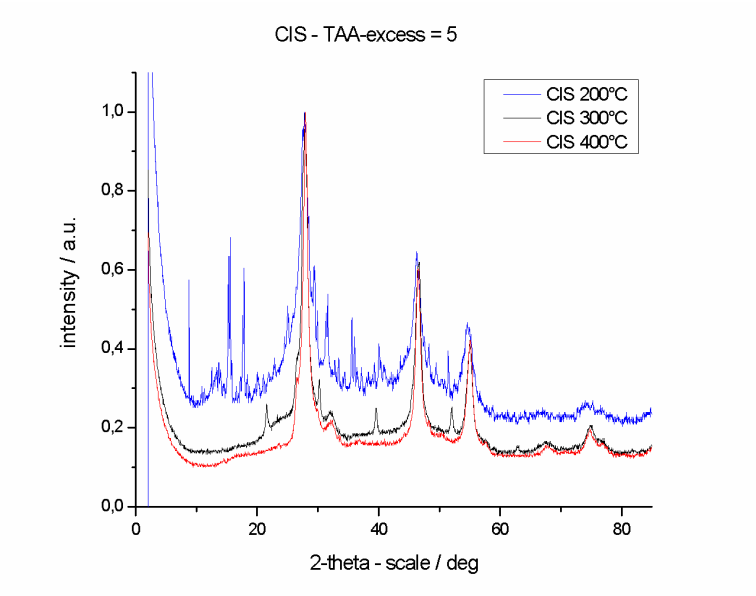

Figure 40: XRD measurements of the $CuInS_2$ layers annealed at different temperatures, showing the impurities within the low tempered layer and very pure layer at 300 °C and 400 °C.

Inverse nanocomposite cells using the above described approach were difficult to produce, as the $CuInS_2$ layers showed poor wetting properties on the ITO electrode. Within many experiments it was not possible to prepare such an inverse nanocomposite solar cell. However, it was possible to obtain bilayer heterojunction solar cells with the common assembly: glass / ITO / P3EBT / $CuInS_2$ / Al. Although the annealing temperature of the $CuInS_2$ layer was only 180 °C, efficiencies of already 0.24% have been obtained. This result demonstrates that inverse nanocomposite solar cells with $CuInS_2$ as inorganic semiconducting acceptor and the polymer P3EBT as organic donor material might be very promising.

If these wetting problems could be solved, for example by using a different solvent or additives like surfactants, this approach might be a very promising one. The inverse assembly allows a larger range of preparation parameters for the preparation of the inorganic layers. Especially, as shown in this work, it would be possible to use higher temperatures that lead to purer inorganic layers with a higher porosity. The inverse assembly, consisting of a porous inorganic layer in combination with a suitable organic donor polymer, is featured with a large donor-acceptor interface, without having dead ends within the photoactive layer and therefore should lead to higher efficiencies. Hence the herein presented approach for the preparation of $CuInS_2$ layers should be followed in future. Further optimisation should be work on improving the wettability of the $CuInS_2$ layer on ITO or by using another transparent electrode material, and in following by optimising the layer thickness.

6 Appendix

6.1 Solar Cell Analysis Tool

During my work for this diploma thesis more than 7000 solar cells were built by students, graduate engineers and laboratory technicians of our team, which is working on nanocomposite solar cells. The most important characteristic of every solar cell is of course the I-V curve and therefore the measuring and analysis of the I-V characteristics is the first analysing step anyway. The measuring itself takes already some time and the analysis even more. The measurement data had to be put into some analysing software, like Origin for instance to get the plots of the I-V curves. This had to be done for each solar cell solar cell including formatting work et cetera. This is not only time-consuming but also quite extensive, if you keep in mind, that each of us built approximately 20-50 solar cells a week. Therefore the idea of creating a tool to facilitate this analysing step and reduce working time was born.

6.1.1 Requirements

As I started thinking about something like an analysis tool seriously I had to think about the requirements on the tool. The tool had to be

- quick,
- easy to use,
- safe concerning data security
- and of course it had to do all the analysis work automatically.

6.1.2 Planning of the Analysis Tool

As Microsoft Excel is a very common tool and furthermore I had already some experiences with it, Excel including VBA was chosen for programming the analysis tool. Rather than I had the idea to enlarge my little project and create a sort of database of all our cells by listing every cell including the most important analysis data in one sheet of the file. More than that, I wanted to include the documentation of the done work as far as possible. Therefore we already used a template, where we had to write in all the parameters of the main steps of the solar cell production and to insert a copy of the I-V curves. So I created an interface from the analysis tool (Excel) to the production

template (Word), which I had to adjust as well and managed to include the documentation that way.

6.1.3 Configuration of the Analysis Tool

The Analysis Tool is located in a folder on a server where everyone of our working group has access. To ensure data security, a backup file is created every day, including a time and date stamp in the file name to be distinctive.

6.1.3.1 The Worksheets

The analysis tool consists of the following four worksheets:

- The Worksheet “Parameter”, where the parameters for the automatic processes, like the paths of the folders and templates to create the backup files and the solar cell production sheets can be typed in and changed as well. The input and the analysis of the data are guided by forms, which can be called up by a button in the worksheet “Solarzellen”. As you can see in Figure 44 some of the input boxes are combined with dropdown lists of some input possibilities. These input options are listed in the worksheet “Parameter” too.
- The Worksheet “Diagramme”, where the I-V curve of the respective solar cell is created and formatted automatically. Afterwards the I-V curves of each solar cell are copied and inserted in the production sheet of the respective type series. The user does not really need to see this worksheet or even change something at it anyhow it is still visible for the user, just to have the possibility to take a look at the graphs during the analysis.
- The Worksheet “Auswertung”, where all the input data from the measurement file of the respective solar cell is transferred to and the calculations take place, that are necessary to get the characteristic data (V_{OC}, I_{SC}, V_{mpp}, I_{mpp}, FF, Eff) of each solar cell. This worksheet is invisible for the user.
- The Worksheet “Solarzellen”, which is the heart of the whole analysis tool. This is always the first sheet the user sees after opening the file; in fact it is the mainsheet. In this sheet all the command buttons to use the tool and its functionality, are located. Actually this is the only sheet the user really needs to see and to use. Here are listed all the solar cells, which have ever been built and analyzed by this tool, including the input data like the used chemicals or the name of the operator as well as the analysing data like V_{OC}, I_{SC} et cetera. Actually this worksheet is a database of all solar cells produced in our working group.

6.1.3.2 The Input Form

For the input of the data, which is used to do the analysis work, I designed an input form which can be called up by clicking a button in the mainsheet of the analysis tool. At this it is compulsory to enter not only the measurement files of the solar cell at dark and illuminated conditions, but also essential data for the calculation of the characteristic points of the I-V curve (V_{OC}, I_{SC}, etc.) like the area of the electrode and the irradiance. The analysis tool has to be fed with metadata like the operator's initials, date, used polymer, and the number of the type series as well. The possibility of input failures can be eliminated by using such a form, which is shown in Figure 41, Figure 42 and Figure 43.

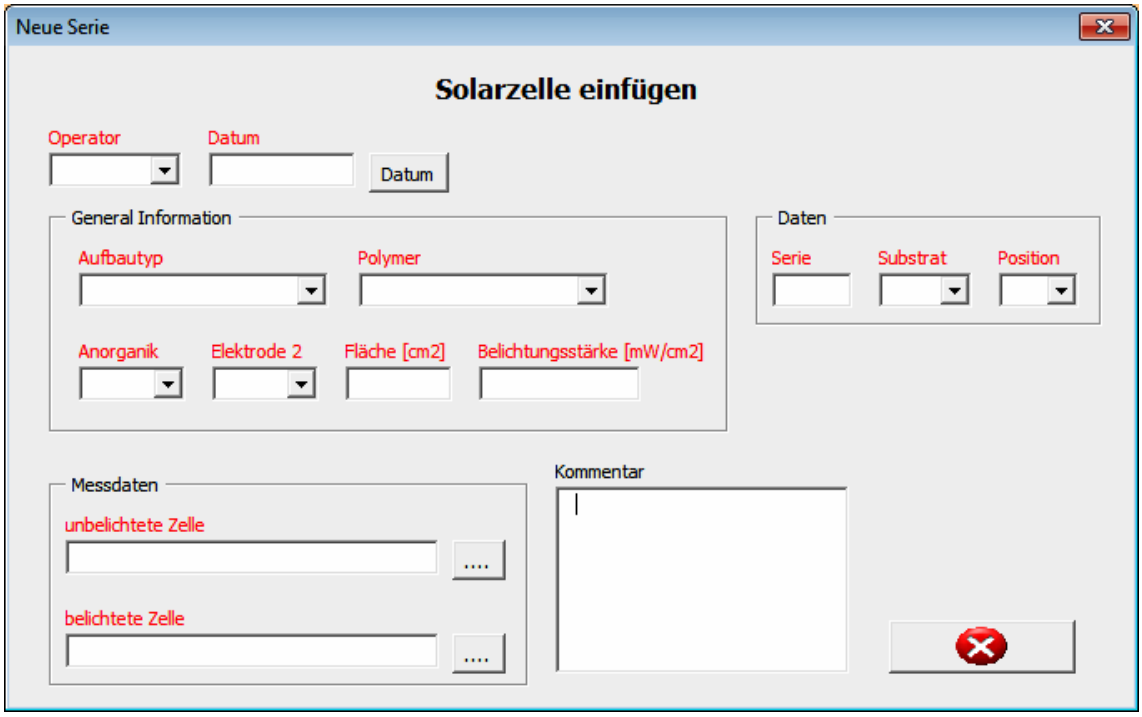

Figure 41: Blank Input Form of the Solar Cell Analysis Tool

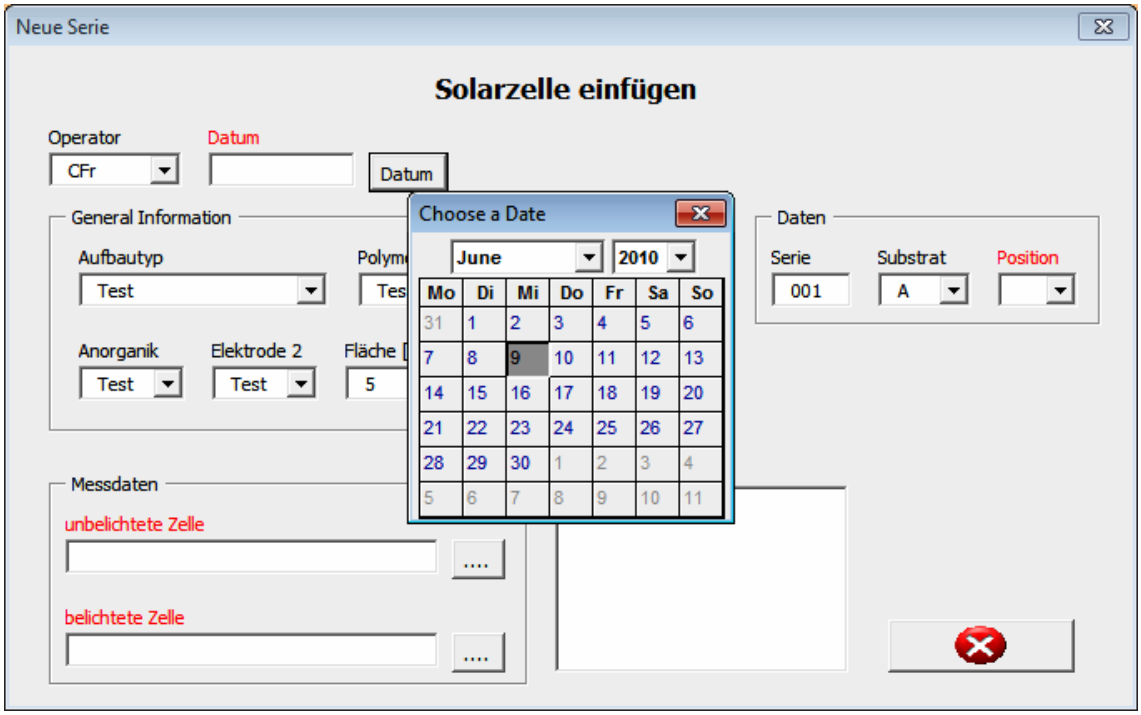

Figure 42: Partially Filled Input Form with Calendar

All the input boxes, except the commentary box, which is optional, are mandatory to be filled as they have a red labelling as long as they are empty. The date can be selected by a calendar (Figure 42) to avoid the usage of different date formats, which would lead to problems in the following analysis process. Not before every mandatory input box is filled with data, the green button appears (shown in Figure 43), which has to be clicked to start the analysis.

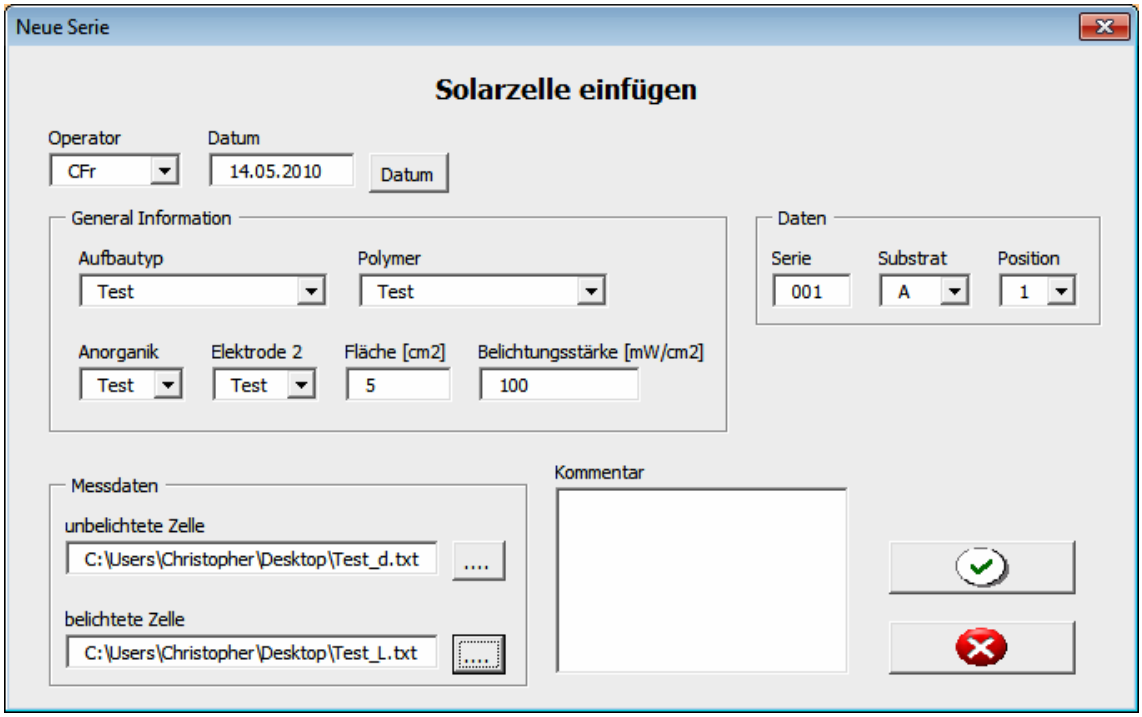

Figure 43: Completely Filled Input Form without Commentary, which is optional

6.1.4 Analysing Process

After pushing the green button the analysis of the first solar cell starts. The Analysis includes

- The import of the measurement files of the solar cell under dark and illuminated conditions
- The plotting of the I-V curve of the solar cell
- The calculation of V_{OC}, I_{SC}, V_{mpp}, I_{mpp}; FF and Eff
- The automatic generation of a solar cell analysis file based on a word template, which contains all the metadata, the I-V curve and the calculated characteristic values of the solar cell
- The adding of this solar cell including its characteristic values and a hyperlink to the corresponding solar cell analysis file, to the database (worksheet “Solarzellen”)

The user has the opportunity to continue the analysing process after the analysis of the first solar cell is done as he has after every single solar cell analysis. This is useful as almost at all times more than just one solar cell is built within one type series. In that case the input form pops up again and the data, which apply for the whole type series, remain stored in the respective text boxes and only the cell specific data has to be typed in again as well as the appropriate measurement files have to be selected (Figure 44). The analysis starts again including the steps listed above, differing by the

fact that the I-V curve and the data are stored in the same solar cell analysis file, which was generated by analyzing the first solar cell, but not in a new one. So there exists one Word file for one type series and this file is linked in the database to every solar cell belonging to that series. Screenshots of the solar cell database (worksheet “Solarzellen”) are shown at Figure 45 and Figure 46. At the end of the analysis of every solar cell the user has the possibility to end the analysis of the type series. Now all the solar cells are listed in the database and solar cell analysis file is saved in a special folder and can be called up by the hyperlink in the database. In addition to that the user can stop the analyzing process at every point by clicking de red button of the input form. In that case the data of all the cells, which have been analyzed in line with this type series before, remain saved in the database and in the solar cell analysis file.

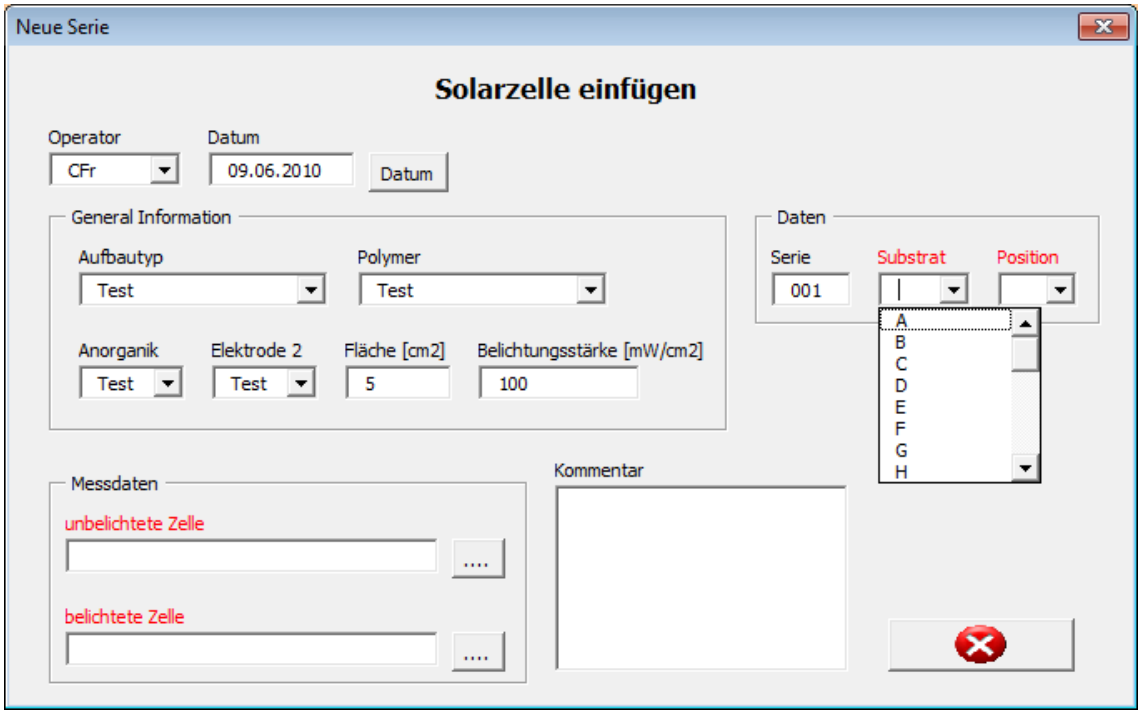

Figure 44: Input Form after the first solar cell has been analyzed and the analysis has been continued. All the input boxes concerning type series information are filled and all the input boxes concerning solar cell specific information are empty.

6.1.5 Solar Cell Database

In the solar cell database every analyzed solar cell is listed including its metadata like date et cetera and its calculated data like open circuit voltage, short circuit current and so on. By using the auto-filter of Excel every column can be filtered, so it is very easy to find a certain dataset, type series or solar cell. This functionality provides the opportunity to limit the displayed solar cells by their assembly, their date of production or their values for V_{OC} or efficiency for instance. The auto-filter is a very well performing tool that raises the functionality and the usability of the database to a higher level.

	A	B	C	D	E	F	G	H	I	J	K	L	M
1	Neue Zelle		Filter aus				Daten						
2	Filename	Person	Datum	Serie	Substrat	Position		Typ	Polymer	Anorg.	Elektr.	Fläche	P_in
1129	CFr_100609_001	CFr	09.06.2010	001	A	1		Bulk-Heterojunction	P3HT	PCBM	Al	10	1,6*10^-5
1130	CFr_100609_001	CFr	09.06.2010	001	A	2		Bulk-Heterojunction	P3HT	PCBM	Al	10	1,6*10^-5
1131	CFr_100609_001	CFr	09.06.2010	001	A	3		Bulk-Heterojunction	P3HT	PCBM	Al	10	1,6*10^-5
1132	CFr_100609_001	CFr	09.06.2010	001	B	1		Bulk-Heterojunction	P3HT	PCBM	Al	10	1,6*10^-5
1133	CFr_100609_001	CFr	09.06.2010	001	B	2		Bulk-Heterojunction	P3HT	PCBM	Al	10	1,6*10^-5
1134	CFr_100609_001	CFr	09.06.2010	001	B	3		Bulk-Heterojunction	P3HT	PCBM	Al	10	1,6*10^-5
1135	CFr_100609_001	CFr	09.06.2010	001	C	1		Bulk-Heterojunction	P3HT	PCBM	Al	10	1,6*10^-5
1136	CFr_100609_001	CFr	09.06.2010	001	C	2		Bulk-Heterojunction	P3HT	PCBM	Al	10	1,6*10^-5
1137	CFr_100609_001	CFr	09.06.2010	001	C	3		Bulk-Heterojunction	P3HT	PCBM	Al	10	1,6*10^-5
1138	CFr_100613_002	CFr	09.06.2010	002	A	1		Inverse BHJ	P3HT	PCBM	Au	10	1,8*10^-5
1139	CFr_100613_002	CFr	09.06.2010	002	A	1		Inverse BHJ	P3HT	PCBM	Au	10	1,8*10^-5
1140	CFr_100613_002	CFr	09.06.2010	002	A	2		Inverse BHJ	P3HT	PCBM	Au	10	1,8*10^-5
1141	CFr_100613_002	CFr	09.06.2010	002	A	3		Inverse BHJ	P3HT	PCBM	Au	10	1,8*10^-5
1142	CFr_100613_002	CFr	09.06.2010	002	B	1		Inverse BHJ	P3HT	PCBM	Au	10	1,8*10^-5
1143	CFr_100613_002	CFr	09.06.2010	002	B	2		Inverse BHJ	P3HT	PCBM	Au	10	1,8*10^-5
1144	CFr_100613_002	CFr	09.06.2010	002	B	3		Inverse BHJ	P3HT	PCBM	Au	10	1,8*10^-5
1145	CFr_100613_002	CFr	09.06.2010	002	C	1		Inverse BHJ	P3HT	PCBM	Au	10	1,8*10^-5
1146	CFr_100613_002	CFr	09.06.2010	002	C	2		Inverse BHJ	P3HT	PCBM	Au	10	1,8*10^-5
1147	CFr_100613_002	CFr	09.06.2010	002	C	3		Inverse BHJ	P3HT	PCBM	Au	10	1,8*10^-5

Figure 45: Screenshot of the solar cell database showing all the metadata of the cells

	A	B	C	D	E	F	G	N	O	P	Q	R	S	T	
1	Neue Zelle		Filter aus				Daten	Auswertung							Kommentar
2	Filename	Person	Datum	Serie	Substrat	Position			V_{OC}	I_{SC}	V_{MPP}	I_{MPP}	FF	η	
1129	CFr_100609_001	CFr	09.06.2010	001	A	1			0,650	1,25E+01	0,410	8,2037	41,6	3,3635	
1130	CFr_100609_001	CFr	09.06.2010	001	A	2			0,650	1,24E+01	0,420	8,0972	42,1	3,4008	
1131	CFr_100609_001	CFr	09.06.2010	001	A	3			0,660	1,27E+01	0,410	8,3862	41,1	3,4384	
1132	CFr_100609_001	CFr	09.06.2010	001	B	1			0,650	1,25E+01	0,410	8,4141	42,5	3,4498	
1133	CFr_100609_001	CFr	09.06.2010	001	B	2			0,650	1,17E+01	0,420	8,3483	46,1	3,5063	
1134	CFr_100609_001	CFr	09.06.2010	001	B	3			0,650	1,18E+01	0,430	8,5536	48,0	3,678	
1135	CFr_100609_001	CFr	09.06.2010	001	C	1			0,660	1,08E+01	0,440	8,1858	50,3	3,6018	
1136	CFr_100609_001	CFr	09.06.2010	001	C	2			0,660	1,13E+01	0,440	8,3036	49,2	3,6536	
1137	CFr_100609_001	CFr	09.06.2010	001	C	3			0,660	1,13E+01	0,440	8,4187	49,8	3,7042	
1138	CFr_100613_002	CFr	09.06.2010	002	A	1			0,600	9,06E+00	0,300	4,786	26,4	1,4802	
1139	CFr_100613_002	CFr	09.06.2010	002	A	1			0,600	9,20E+00	0,300	4,8345	26,3	1,4952	2. Messung
1140	CFr_100613_002	CFr	09.06.2010	002	A	2			0,500	1,10E+01	0,260	5,898	28,0	1,5809	
1141	CFr_100613_002	CFr	09.06.2010	002	A	3			0,500	1,15E+01	0,260	6,1909	28,0	1,6594	
1142	CFr_100613_002	CFr	09.06.2010	002	B	1			0,600	1,33E+01	0,320	7,15	28,7	2,3588	
1143	CFr_100613_002	CFr	09.06.2010	002	B	2			0,600	1,37E+01	0,320	7,585	29,6	2,5023	
1144	CFr_100613_002	CFr	09.06.2010	002	B	3			0,600	1,50E+01	0,310	8,1293	28,0	2,598	
1145	CFr_100613_002	CFr	09.06.2010	002	C	1			0,600	1,05E+01	0,300	5,5362	26,3	1,7122	
1146	CFr_100613_002	CFr	09.06.2010	002	C	2			0,600	1,07E+01	0,300	5,6252	26,3	1,7398	
1147	CFr_100613_002	CFr	09.06.2010	002	C	3			0,600	1,37E+01	0,310	7,0664	26,7	2,2583	

Figure 46: Screenshot of the solar cell database showing all the analysis data of the cells

6.1.6 Effect of the Analysis Tool on the Daily Work

The employment of this solar cell analysis tool in our working group helped a lot to facilitate the interpretation, the reporting and the documentation of our work. The analysis of a whole type series takes us less than five minutes by using the tool. Beforehand it took us at least half an hour to analyse the same amount of solar cells. It took us even longer to do all the formatting work and the documentation, which are now included in the analysing process. As the database itself forms already a completely new and very useful tool and the I-V curves of the solar cells that are generated automatically, can easily be used for smaller presentations or written reports as well, there follows even more saving of labour from the use of the solar cell analysis tool altogether.

6.2 Details on the used Chemicals

2 - Propanol

Hazard Symbols: F, Xi

Form: Liquid, colourless

Molecular Formula: C_3H_8O, Molecular Weight: 60.01 $gmol^{-1}$

Density: 0.785 gml^{-1}, Boiling point: 82 °C, Ignition Temperature: 425 °C

Acetone

Hazard Symbols: F, Xi

Form: Liquid, clear, colourless

Molecular Formula: C_3H_6O, Molecular Weight: 58.08 $gmol^{-1}$

Density: 0.791 gml^{-1}, Boiling point: 56 °C, Ignition Temperature: 465 °C

Aluminium

Molecular Formula: Al, Molecular Weight: 26.98 $gmol^{-1}$

Density: 2.1 gml^{-1}, Melting point: 660.37 °C

Chloroform

Hazard Symbols: Xn

Form: Liquid, clear, colourless

Molecular Formula: $CHCl_3$, Molecular Weight: 119.38 $gmol^{-1}$

Density: 1.492 gml^{-1}, Boiling point: 60.5 – 61.5 °C

Copper (I) iodide

Hazard Symbols: Xn, N

Form: powder, brown, odourless

Molecular Formula: CuI, Molecular Weight: 190.45 $gmol^{-1}$

Density: 5.62 gml^{-1}, Melting point: 605 °C

Copper (I) acetate

Hazard Symbols: Xi

Form: solid

Molecular Formula: $C_2H_3CuO_2$, Molecular Weight: 122.59 $gmol^{-1}$

Melting point: 250 °C

Gold

Molecular Formula: Au, Molecular Weight: 196.97 $gmol^{-1}$

Density: 19.3 gml^{-1}, Melting point: 1063 °C

Hydrochlorid Acid

Hazard Symbols: C

Form: liquid, light yellow, pungent

Molecular Formula: HCl, Molecular Weight: 36.46 $gmol^{-1}$

Density: 1.2 gcm^{-3}, Boiling point: 110 °C

Vapour pressure: 227 hPa (21.1 °C), 547 hPa (37.1 °C)

Indium (III) chloride

Hazard Symbols: C

Form: powder

Molecular Formula: $InCl_3$, Molecular Weight: 221.18 $gmol^{-1}$

Density: 3.46 gml^{-1}

P3EBT

IUPAC name: Poly[3-(ethyl-4-butanoate)thiophene-2,5-diyl]

Form: solid, dark violet

Molecular Formula: $C_{10}H_{12}O_2S$

Further properties: 90% - 93% regioregularity

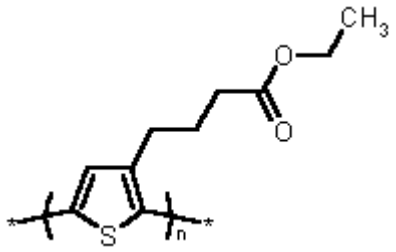

Figure 47: Chemical structure of P3EBT

P3HT

IUPAC name: Poly(3-hexylthiophene-2,5-diyl)

Form: solid, dark purple

Molecular Formula: $C_{10}H_{14}S$,

Further properties: regioregular,

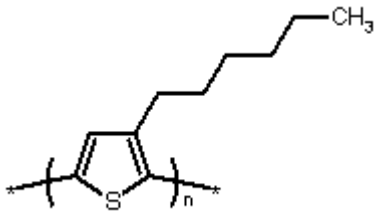

Figure 48: Chemical structure of P3HT

PCBM

Hazard Symbols: Xi

Form: black to light brown, solid and/or crystal

IUPAC name: [6,6]-Phenyl C61 butyric acid methyl ester 1-[3-(methoxycarbonyl)propyl]-1-phenyl-[6.6]C61 3'H-cyclopropa[1,9][5,6]fullerene-C60-Ih-3'-butanoic acid 3'-phenyl methyl ester

Molecular Formula: $C_{72}H_{14}O_2$, Molecular Weight: 910.9 $gmol^{-1}$

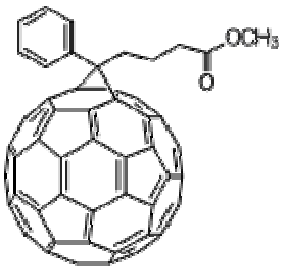

Figure 49: Chemical structure of PCBM [60]

Pyridine

Hazard Symbols: F, Xn

Form: Liquid, colourless, unpleasant odour

Molecular Formula: C_5H_5N, Molecular Weight: 79.1 $gmol^{-1}$

Density: 0.978 gcm^{-3}, Boiling point: 115 °C, Ignition Temperature: 482 °C

Thioacetamide

Hazard Symbols: T

Form: crystalline, white

Molecular Formula: C_2H_5NS, Molecular Weight: 75.13 $gmol^{-1}$

Melting point: 108 - 112 °C

Thiourea

Hazard Symbols: Xn, N

Form: crystalline, white, odourless

Molecular Formula: CH_4N_2S, Molecular Weight: 76.12 $gmol^{-1}$

Density: 1.405 gcm^{-3}, Melting point: 170 - 176 °C

Titanium

Molecular Formula: Ti, Molecular Weight: 47.87 $gmol^{-1}$

Density: 4.5 gml^{-1}, Melting point: 1660 °C

Zinc acetate

Hazard Symbols: Xn, N

Form: solid

Molecular Formula: $C_4H_6O_4Zn$, Molecular Weight: 183.48 $gmol^{-1}$

Density: 1.84 gml^{-1}

Zinc chloride

Hazard Symbols: C, N

Form: crystalline, powder, white

Molecular Formula: $ZnCl_2$, Molecular Weight: 136.28 $gmol^{-1}$

Density: 2.907 gcm^{-3}, Melting point: 293 °C

Zinc powder

Hazard Symbols: F, N

Form: powder

Molecular Formula: Zn, Molecular Weight: 65.39 $gmol^{-1}$

Density: 7.133 gml^{-1}, Melting point: 420 °C

6.3 List of Abbreviations

χ_{Ea}	Electron affinity of the acceptor
χ_{Ed}	Electron affinity of the donor
a.u.	Arbitrary units
AM	air mass
BHJ	bulk heterojunction
CF	chloroform
CIS	copper indium disulfide
d	film thickness
d_{layer}	Average layer thickness
D_{XRD}	diameter of the primary crystallites determined by XRD-analysis
E_{ex}	exciton energy
eq.	equivalents
EQE	external quantum efficiency
eV	Electron volt
FF	fill factor
HOMO	highest occupied molecule orbital
I	Current
I_{mpp}	circuit at the maximum power point
IPCE	Incident photon to current efficiency
IP_d	ionization energy of the donor
I_{SC}	short circuit current
ITO	indium tin oxide
LUMO	lowest unoccupied molecule orbital
P3HT	Poly(3-hexylthiophene-2,5-diyl)
PCBM	[6,6]-Phenyl C61 butyric acid methyl ester
PEDOT:PSS	Poly(3,4-ethylenedioxythiophene) : poly(styrenesulfonate)
P_{in}	Incident light power
P_{max}	maximum power point

SEM	scanning electron microscopy
T	temperature
TAA	thioacetamide
THS	Thiourea
V	Voltage
V_{mpp}	voltage at the maximum power point
V_{OC}	open circuit voltage
XRD	X-ray diffraction
ZnAc	zinc acetate
η	efficiency
η_e	power conversion efficiency
θ	angle (X-ray diffraction)
λ	wavelength
σ	standard deviation

6.4 List of Tables

6.5 List of Figures